THESIS

VERTICAL DISTRIBUTION OF WATER VAPOR USING SATELLITE SOUNDING METHODS WITH NEW AIRCRAFT DATA VALIDATION

Submitted by
Brian D. McNoldy
Department of Atmospheric Science

In partial fulfillment of the requirements
for the Degree of Master of Science
Colorado State University
Fort Collins, Colorado
Summer 2001

COLORADO STATE UNIVERSITY

April 23, 2001

WE HEREBY RECOMMEND THAT THE THESIS PREPARED UNDER OUR SUPERVISION BY BRIAN D. MCNOLDY ENTITLED VERTICAL DISTRIBUTION OF WATER VAPOR USING SATELLITE SOUNDING METHODS WITH NEW AIRCRAFT DATA VALIDATION BE ACCEPTED AS FULFILLING IN PART REQUIREMENTS FOR THE DEGREE OF MASTER OF SCIENCE.

Committee on Graduate Work

_____

_____

_____

_____

_____

Adviser

_____

Department Head

ABSTRACT

VERTICAL DISTRIBUTION OF WATER VAPOR USING SATELLITE SOUNDING METHODS WITH NEW AIRCRAFT DATA VALIDATION

The importance of water vapor in Earth's climate system is undisputedly immense. Its meteorological impacts range from radiative transfer to the hydrologic cycle, on scales ranging from local to planetary. It affects military operations, commercial flights, and private industry. However, global measurements of water vapor can currently only be obtained from satellites, since ground stations are sparse and ocean stations are nearly non-existent. Unfortunately, the satellites cannot directly measure water vapor; instead, they detect radiation at discrete frequencies. The signals originate from different altitudes in the atmosphere, providing vertical resolution. A complex mathematical inversion is necessary to retrieve the desired quantity (water vapor) from the measured quantity (brightness temperatures). Both the satellite calibration and the retrieval algorithm contribute to errors in the retrieved parameters.

The focus here is on the validation of a satellite-based retrieval using *in-situ* measurements of water vapor made by commercial aircraft. The Aircraft Communications Addressing and Reporting System (ACARS) routinely records a plethora of meteorological parameters, including temperature, pressure, wind velocities, and turbulence. The new Water Vapor Sensing System (WVSS) added water vapor mixing ratio and dewpoint to the array of parameters. These measurements will be compared to the humidity measurements retrieved from the satellite-based TIROS

Operational Vertical Sounder (TOVS) High-resolution Infrared Radiation Sounder (HIRS) radiances over the continental United States.

This study shows that the water vapor retrieval algorithm is approximately 20% too dry through most of the atmosphere when compared to aircraft measurements of the same parameter.

Brian D. McNoldy

Department of Atmospheric Science

Colorado State University

Fort Collins, Colorado 80523-1371

Summer 2001

ACKNOWLEDGEMENTS

Many thanks to my advisor, Dr. Thomas Vonder Haar, and committee members Dr. Graeme Stephens in the Atmospheric Science Department and Dr. Chiao-Yao She in the Physics Department. Their input has been invaluable and their time is greatly appreciated. I would also like to thank the entire Vonder Haar research group.

Much of this work would not have been possible without the help of John Forsythe at the Cooperative Institute for Research in the Atmosphere; Richard Engelen at Colorado State University; Rex Fleming at the University Corporation for Atmospheric Research; and John Bates and Darren Jackson at the National Oceanic and Atmospheric Administration's Environmental Technology Laboratory. Also, Robert Fleishauer, Robert LeeJoice, and Larry Belcher provided priceless interaction, discussion, and guidance.

This research was supported by the *Water Vapor in the Climate System Project*, NASA Grant NAG5-3449; the *CloudSat Program*, NASA Grant NAS5-99237; and the *United States Department of Defense Center for Geosciences / Atmospheric Research*, Cooperative Agreement DAAL01-98-2-0078.

Table of Contents

1. Introduction

Water vapor plays a fundamental role in the transfer of energy and moisture in the atmosphere. Only since the advent of the satellite in the 1950's has it been quantitatively measured on a global scale. Recent developments in satellite instrumentation have dramatically increased the resolution and accuracy of such measurements. However, to say that satellites directly measure water vapor is too broad a statement. Instead, they are only capable of measuring the radiation emitted (brightness temperature, or equivalent blackbody temperature) at frequencies where water vapor is weakly and strongly absorbing.

Basically, to gain information about water vapor, an inverse relationship must be utilized; that is, given a brightness temperature as a function of water vapor, retrieve water vapor as a function of brightness temperature. This method leaves room for errors and non-unique solutions.

Recent applications of an optimum estimation retrieval have been tested, but primarily against other satellite-based climatologies (Engelen and Stephens 1999, Stephens et al 1996, Susskind et al 1984; Vonder Haar et al 1999). Other validation attempts have been made via inter-satellite comparisons (Berg et al 1999, Bréon et al 2000, Engelen and Stephens 1998, Engelen and Stephens 1999, Susskind et al 1997) and radiosondes (Jackson and Stephens 1995, Smith 1991). Early work by Newell (2000) strives to validate satellite data with aircraft measurements, but much of that work is unpublished. An independent *in-situ* method of validation would be valuable to assure the results from the retrievals are accurate. Radiosondes can only partially fulfill this need; their distribution is sparse over land and nearly non-existent over oceans and

uninhabited areas. This study uses measurements of water vapor made by instruments on commercial aircraft to validate the retrieval described by Clive Rodgers (1976).

Aircraft measurements of meteorological parameters are not a new development; such activities have been going on since the early 1930's. However, due to underdeveloped aircraft technology at the time, this was very dangerous and resulted in the loss of a dozen pilots; the program was terminated after only ten years. In the late 1970's, routine observations were again being made, this time by commercial aircraft. The Aircraft Communications Addressing and Reporting System (ACARS) allows for reliable air-to-ground digital telecommunications. The addition of water vapor parameters came about with the Water Vapor Sensing System (WVSS) in 1996 (Fleming 1996). The ACARS network now receives over 50,000 reports per day from commercial aircraft.

1.1 Satellite Sounding Methods

Satellite sounding methods are all based on the fact that different gases absorb and emit radiation differently. In the case of water vapor, most of the gas is concentrated near the surface, but the smaller amounts in the middle and upper troposphere are still significant for radiative transfer and global climate feedback.

The "shape" of a molecule is defined by the atomic composition. Water vapor is a tri-atomic molecule and is capable of various rotations and vibrations. These motions are a function of the energy of the molecule; its characteristics therefore change as the frequency of the incident or emitted radiation is changed. Figure 1.1 shows that the atmosphere's absorption spectrum is dominated by the effects of the water vapor molecule at infrared wavelengths (Stephens 1994).

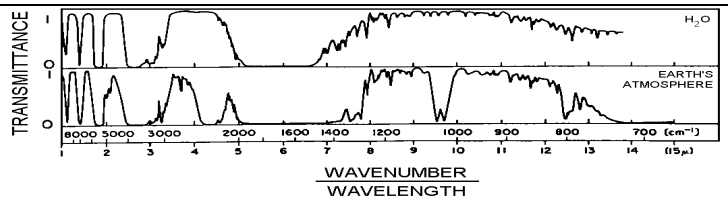

Fig. 1.1. The infrared absorption spectrum of water vapor (top) and of the entire atmosphere (bottom) (Stephens 1994).

A "weighting function" is used to more accurately retrieve radiances as a function of altitude. Weighting functions characterize the scale height of the absorbing gas as well the optical depth, allowing the radiances received by the satellite to be properly discriminated by their altitude of emission. The weighting functions also depend on the temperature and mixing ratio of a gas as a function of altitude. Figure 1.2 shows weighting functions for four channels of the TOVS HIRS sensor (details follow in Section 2.2). Channel 8 is centered at 11.1 μm and is most sensitive to thermal radiation emitted by the surface. Channels 10, 11, and 12 (8.2 μm, 7.3 μm, 6.7 μm) are sensitive to lower, middle, and upper-tropospheric water vapor, respectively.

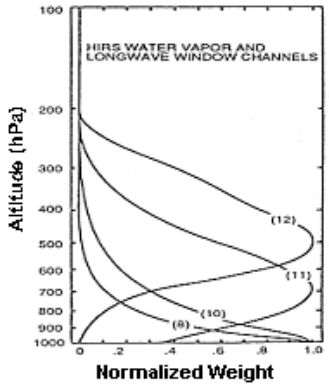

Fig. 1.2. Weighting functions for four channels of the TOVS HIRS instrument. Notice how the altitude of peak sensitivity changes as the frequency of the channel changes (Stephens 1994).

Weighting functions are used to characterize the amount of a gas in the atmosphere, that is, how the transmission properties vary with altitude. They typically grow exponentially from the surface to some height z_{MAX} (height of peak sensitivity), then decay exponentially from z_{MAX} to the top of the atmosphere. This behavior accounts for the decrease in amount of the absorbing gas and the increase in transmission with altitude. Simplified weighting functions can be mathematically described by

$$W = \frac{2}{H}\exp\left[\frac{2z_{\max}}{H} - \frac{2z}{H} - \exp\left(\frac{2z_{\max}}{H} - \frac{2z}{H}\right)\right], \tag{1.1}$$

where W is the weighting function, z_{MAX} is the altitude at which W peaks, z is some arbitrary altitude, and H is the atmospheric scale height. An alternate version looks like

$$W = \frac{2\tau^*}{H}\exp\left[-\frac{2z}{H} - \tau^* \exp\left(-\frac{2z}{H}\right)\right], \tag{1.2}$$

where τ^* is the total optical depth of the atmosphere. The peak of the weighting function occurs where τ^* is largest. Weighting functions that peak higher or lower than z_{MAX} are broader and do not describe the gas distribution as well (poorer vertical resolution). As the absorption coefficient falls off exponentially away from this optical depth maximum, so does the weighting function.

Weighting functions are used to analyze the radiation received by satellites so that the altitude (z) from where the radiances were emitted can be identified. Given $W(z, \infty)$, the resulting radiance equation for a nadir sounding may look like the following:

$$I(\infty) = I(0)T(0,\infty) + \int_0^\infty B(z)W(z,\infty)dz\,, \tag{1.3}$$

where $I(\infty)$ is the intensity measured at the satellite's altitude (basically, very large z); $I(0)$ is the intensity received from the ground, weighted by the transmission through the

atmosphere $T(0,\infty)$; and $B(z)$ is the Planck blackbody emission at some height z, weighted by the weighting function through the layer $W(z,\infty)$ (Stephens 1994).

The $I(\infty)$ described above is the raw data that ground stations download from the satellite. In that form, it is not very meaningful to most people, but if those radiances can be translated into useful products such as surface temperature, cloud-top temperature, or water vapor concentrations, the data is suddenly very useful to many people. That translation is accomplished through the use of a retrieval algorithm.

1.2 Satellite-based Water Vapor Retrievals

The basis of retrieval theory is inverting measurements of atmospheric emitted radiation to gain information about the thermal and chemical state of the atmosphere. Unfortunately, this inversion can yield non-unique solutions, that is, several possible states could correspond to the same measured radiances. To help eliminate the mathematical ambiguity, an estimation technique is utilized whereby *a priori* information is used to find the best or most likely solution (Rodgers 1976). This would typically be a climatological mean value of some quantity at a given time and place.

The principal advantage of relying on satellite data is the spatial resolution. A polar-orbiting satellite views approximately the same spot on the Earth twice per day. This includes places over the oceans, deserts, mountains, and other locations where physical observations are either sparse or non-existent. Radiosondes are launched twice per day, matching the temporal resolution of a polar-orbiting satellite; however, there are only about 1500 radiosonde sites scattered across the globe, so the spatial resolution is much worse.

Unfortunately, this high spatial resolution comes at the cost of accuracy. It is no easy task to determine how accurate the instruments on a satellite are once they are in

space. Furthermore, of great interest to this study is how well the transmitted data is manipulated to yield products useful to the scientific community. Assuming the data received on the ground is correct (no satellite or electronic errors), there is still a long way to go before that raw data is molded into something more meaningful… such as the amount of water vapor in a given layer of the atmosphere.

There are mathematical ways to evaluate how well a retrieval performs, but these are simply more manipulation of the satellite data. An ideal way to evaluate a retrieval algorithm would be to use actual measurements of the desired parameter and compare them against the satellite retrieval results.

1.3 Aircraft Measurements of Water Vapor

Measurements of water vapor have been attempted for decades, using balloon radiosondes and satellites. The radiosondes are comparatively cheap, but perform poorly at moisture extremes (very dry or very moist); satellites have good horizontal resolution, but poor vertical resolution, and are not guaranteed to be accurate (Fleming and Braune 2000).

As mentioned earlier, meteorological parameters were first measured by aircraft in the 1930's, but that was largely unsuccessful and very dangerous. In the late 1970's, ACARS (Aircraft Communications Addressing and Reporting System) allowed commercial aircraft to routinely measure some parameters, but not moisture. It was only in 1996, with the introduction of the WVSS (Water Vapor Sensing System), that the first routine measurements of moisture (dewpoint and mixing ratio) were made by commercial aircraft. Details on these data will be discussed later in Section 2.4.

There are many advantages to obtaining *in situ* measurements of water vapor. The key advantage, and the one most relevant to this study, is the validation of a satellite-based retrieval. However, the high temporal and spatial resolution of these data allows

airport crews to make icing forecasts and it allows weather forecasters to improve predictions of cloud formation and rainfall potential in nearly real-time. The data can even be used as input to computer forecast models, such as the National Meteorological Center's Rapid Update Cycle (RUC) model, or the model run by the European Centre for Medium Range Weather Forecasts (ECMWF) (Benjamin et al 1995, Lorenc et al 1996).

The instrument used in the WVSS program is the Vaisala thin-film capacitor. This instrument is actually very similar to the one used on many radiosondes, but is more permanent, rugged, and accurate (Fleming 1999, Fleming and Braune 2000). It is a low-maintenance instrument, so airport crews do not have to concern themselves with it very often, and it is built to withstand high speeds and hostile conditions, while still providing accurate data.

A fundamental difference between measurements made by a radiosonde and measurements made by an aircraft is the temperature at which the instrument operates. Balloon-borne radiosondes perform very poorly at cold temperatures, such as those found in the upper troposphere. A commercial aircraft at flight level travels at roughly 280 m/s; this higher speed is actually advantageous to measurements of moisture. The thin-film capacitor has a finite response time. That is, the instrument cannot record rapid changes in moisture perfectly, but requires some time to adjust to a new environment. The capacitor responds less rapidly at lower ambient temperatures; therefore, the dynamic heating (on the order of 25°C) caused by the aircraft's high speed allows for more accurate moisture measurements and shorter response times. This temperature-speed relationship is stated below:

$$T_T = T_A\left(1 + 0.2M^2\right), \tag{1.4}$$

where T_T is the total temperature, T_A is the ambient temperature, and M is the Mach Number. On the other hand, the ascent rate of a weather balloon is slow enough that

dynamic heating does not occur, so as the balloon reaches higher (colder) altitudes, and the radiosonde performs more poorly. The result is that the balloon capacitors respond about five times slower than the aircraft capacitors at flight level (Fleming and Braune 2000).

With this confidence in place, it is easy to see why aircraft measurements of moisture parameters can be used as “truth” for satellite-based retrieval validation.

1.4 The Need for Retrieval Validation

As hinted at in the previous three sections, neither satellites nor retrieval algorithms are perfect. If they are to be used, they need to be validated at some point to assure their trustworthiness. Although aircraft-borne instruments are not perfect either, their in-flight characteristics can be better determined, so even if they are not working correctly, the error can be traced rather quickly. This is not the case with an instrument on a satellite in space. Access to the satellite is expensive because, at this point, fixing a malfunctioning instrument requires writing and transmitting corrective computer code, or for a serious hardware failure, the instrument is typically decommissioned.

Since this study is not on electrical engineering, optical systems, or orbital mechanics, it will be assumed that the satellite is functioning correctly. That leaves the retrieval algorithm in question. Commercial aircraft measurements of moisture parameters will be compared against satellite observations of the same parameters. With the aircraft measurements held as “truth”, any offsets, biases, or errors in the retrieval algorithm (satellite observations) will be identified. Although the exact portion of the potentially erroneous algorithm cannot be identified, it’s error characteristics can be identified (i.e., less accurate in lower troposphere, biased too high everywhere, etc.).

2. Data

This chapter will discuss the data sources utilized, their error properties, and their contribution to the study. The first two sections focus on the remote sensing aspect: the instruments responsible for making the space-based observations. The third section describes the dataset that was used as *a priori* data for the retrieval; a monthly-average composite of ground-based and space-based observations. The last section of this chapter covers the *in-situ* data used; the aircraft-based measurements that confirm the validity of, and check for potential biases in, the retrieval.

2.1 TIROS Operational Vertical Sounder (TOVS)

TOVS (TIROS (Television and Infrared Observational Satellite) Operational Vertical Sounder) has been onboard the NOAA polar-orbiting satellites since 1978. It is an instrument package consisting of three radiometers: the MSU (Microwave Sounding Unit), the SSU (Stratospheric Sounding Unit), and the HIRS (High Resolution Infrared Radiation Sounder). The data used in this study were collected from the NOAA-J (renamed NOAA 14 after successful launch) satellite, launched in late December of 1994 and still in operation today.

The TIROS-N series of satellites began in 1978 and ended in 1983, at which point the Advanced TIROS-N (ATN) series were utilized (1983-2000+). The ATN series added a few instruments, as well as some channels, to certain pre-existing instruments. Fortunately, there were no notable changes to the TOVS package, thus maintaining the longest climatology possible without instrument changes or data gaps. A brief overview

of each of the TOVS instruments will be presented, followed by a more in-depth look at HIRS (Section 2.2), which is of particular interest to this study.

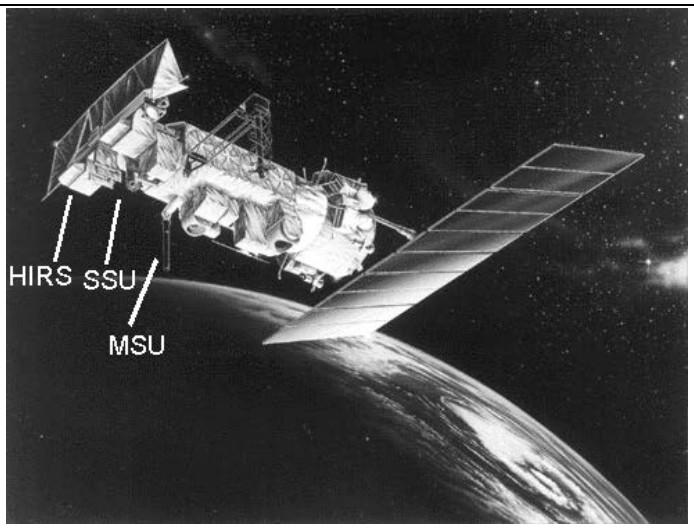

Fig. 2.1 A painting of the NOAA J (NOAA 14) satellite in orbit. The three TOVS instruments are labeled (Image courtesy of NOAA NESDIS).

2.1.1 The Microwave Sounding Unit

The MSU is a scanning microwave radiometer designed to produce tropospheric soundings. The scanning is cross-track, with roughly 170-km resolution and a swath width of nearly 105°.

The current MSU is modeled after the SCAMS (Scanning Microwave Spectrometer) which flew on the Nimbus 6 satellite in 1975. The MSU has four channels, ranging in wavelength from 5.17 to 5.96 mm. Due to the long wavelength at which it senses, it can see through clouds and therefore retrieve temperature soundings in clear or cloudy areas. However, the long wavelength also limits its resolution (Kidder and Vonder Haar 1995).

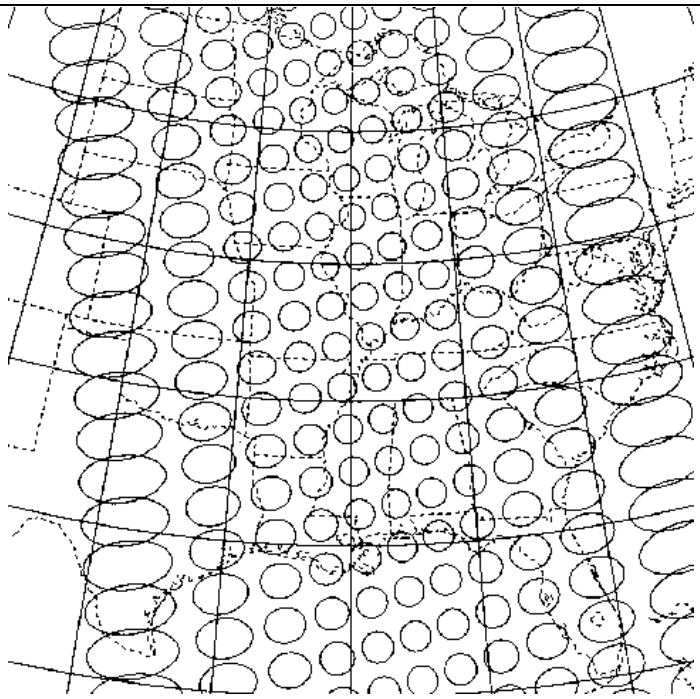

Fig. 2.2 The MSU scan pattern (Kidder and Vonder Haar 1995).

2.1.2 The Stratospheric Sounding Unit

Like the MSU, the SSU is a scanning radiometer, but the SSU senses in the infrared and is designed to produce stratospheric soundings. The scanning is cross-track with roughly 210-km resolution and a swath width of 70°.

The current SSU is modeled after the PMR (Pressure Modulator Radiometer) which also flew on the Nimbus 6 satellite. The SSU has three channels, ranging in wavelength from 14.925 to 14.940 μm.

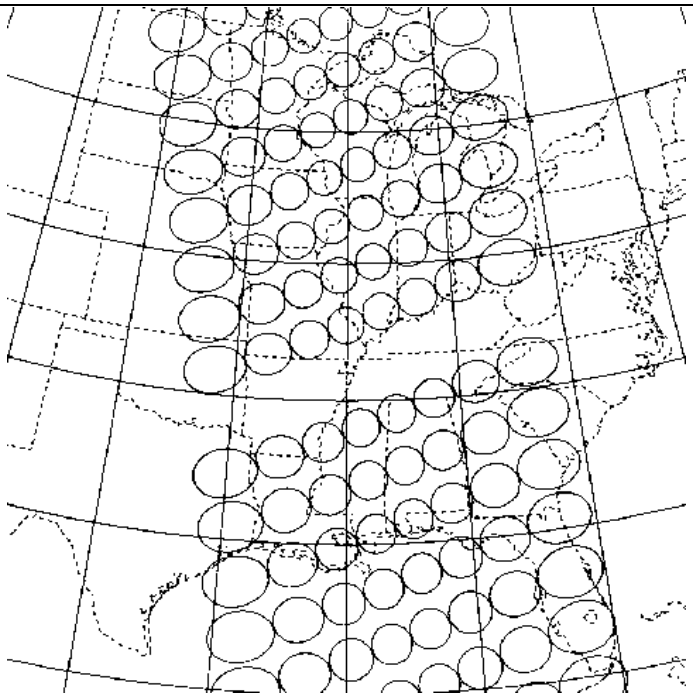

Fig. 2.3 The SSU scan pattern (Kidder and Vonder Haar 1995).

2.1.3 The High-Resolution Infrared Radiation Sounder

This instrument will not be discussed at length here, but details can be found found in Kidder and Vonder Haar (1995). However, the scan pattern is shown just for comparison in Figure 2.4. Notice the higher resolution compared to the other two instruments. This resolution is necessary to capture the fine-scale structures that water vapor exhibits. Newell (2000) observes that water vapor inhomogeneities are “often advected in long filaments that act like rivers”.

Since this was the primary instrument used in the satellite portion of this study, a separate section is devoted to it. Section 2.2 will provide details on the instrument and the data used as input into the water vapor retrieval.

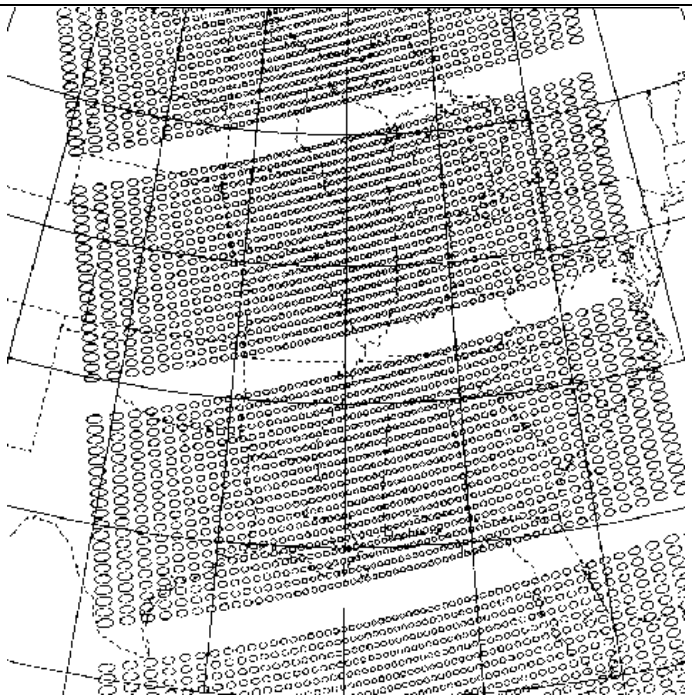

Fig. 2.4 The HIRS/2 scan pattern (Kidder and Vonder Haar 1995).

2.2 High-Resolution Infrared Radiation Sounder (HIRS/2)

The HIRS/2 is a scanning radiometer designed to produce tropospheric soundings of various gases. The instrument scans cross-track with roughly 42-km resolution and a swath width of 99°.

The current HIRS/2 is modeled after the HIRS/1 that flew on the Nimbus 6 satellite in 1975, along with the SCAMS and PMR. The HIRS/2 has twenty channels, ranging in wavelength from 0.69 to 14.95 μm. This large range of wavelengths allows it to view radiation emitted by carbon dioxide, ozone, water vapor, visible, and the surface.

One may notice the peculiar scan pattern (see Figure 2.4). Each scan line is composed of 56 scan steps, but there are always three missing lines after every twenty lines. The reason for the missing lines is calibration. After performing twenty scan lines

looking at the Earth, HIRS/2 enters a calibration mode. When in this mode, the sensor compares space with an internal hot calibration source and then an internal cold calibration source (Kidder and Vonder Haar 1995).

The HIRS/2 data used in this study were provided by John Bates and Darren Jackson at the NOAA Environmental Technology Laboratory (NOAA/ETL) in Boulder, Colorado. The ascending and descending passes of NOAA-14 were averaged together to create a single, daily composite file. The radiances from all twenty channels were cloud-cleared using the method described in Rossow and Garder (1993). The cloud-cleared radiances were then limb-corrected using a multiple regression technique.

At the time of writing, the only recent data available from NOAA/ETL was August 1999. TOVS/HIRS data is being processed there in a chronological fashion, beginning with 1978, so special accommodations were made to process the data for this study. In the future, it would be very beneficial to utilize more data (different months) in the validation.

Since the HIRS/2 data serves as input into the retrieval, its error characteristics will be discussed later in Chapter 5, along with the results. However, some examples of the HIRS/2 water vapor data will be shown here. It must be noted that the figures here do not show the raw radiances, but rather the result of the radiances used as input into the retrieval. The retrieval will be described in detail in Chapter 3.

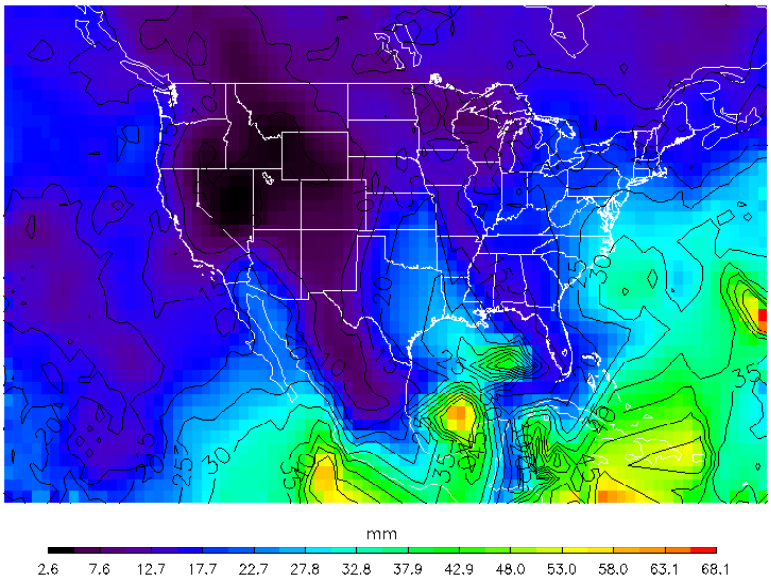

Fig. 2.5 Precipitable water in the 1000-700 hPa layer on August 26, 1999 from the HIRS/2 water vapor retrieval. The large feature near the Greater Antilles is Hurricane Dennis and the concentrated feature near the Yucatan Peninsula is a developing disturbance near the Inter-tropical Convergence Zone.

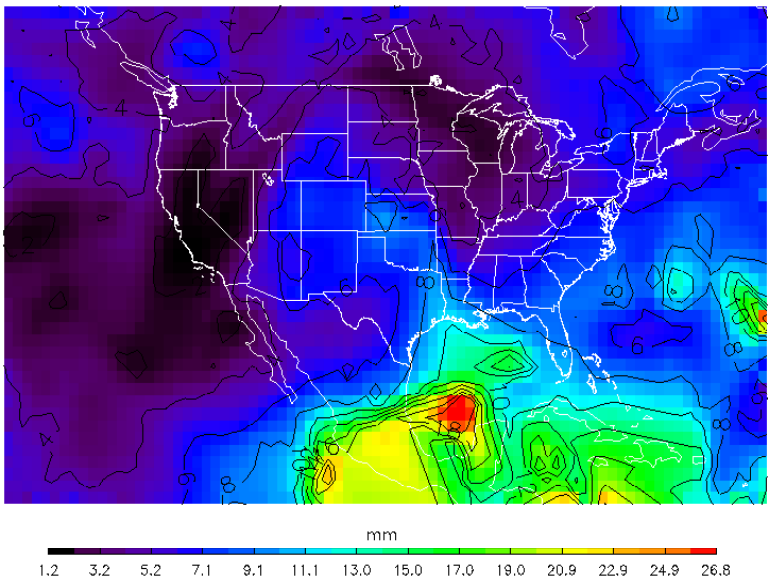

Fig. 2.6 Precipitable water in the 700-500 hPa layer on August 26, 1999 from the HIRS/2 water vapor retrieval.

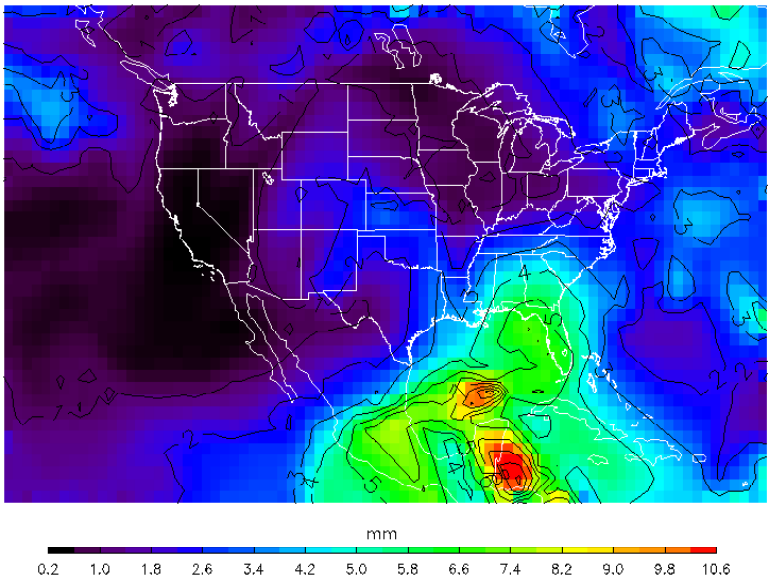

Fig. 2.7 Precipitable water in the 500-300 hPa layer on August 26, 1999 from the HIRS/2 water vapor retrieval.

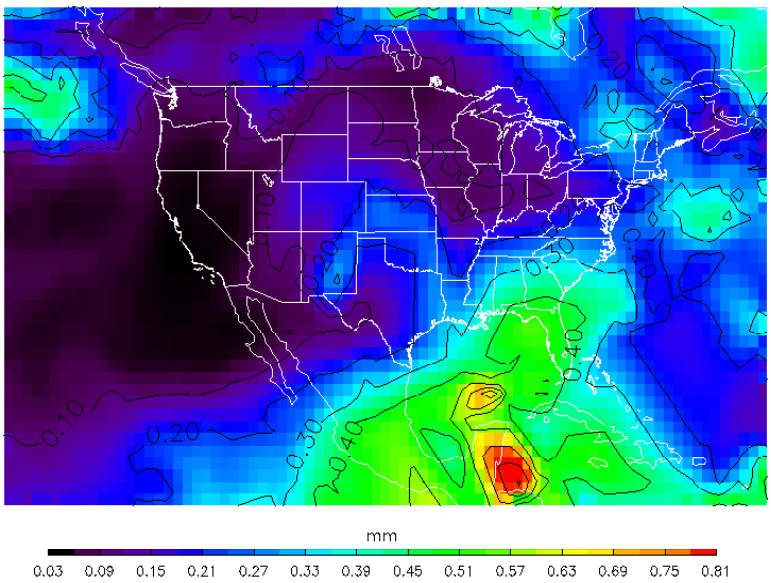

Fig. 2.8 Precipitable water in the 300-200 hPa layer on August 26, 1999 from the HIRS/2 water vapor retrieval.

Notice that the retrieval produces water vapor data in four layers and that the data is displayed in the original 1° bins. The *a priori* data used will be described in Section 2.3 and is the basis of the 1° resolution.

2.3 NASA Water Vapor Project (NVAP)

The NASA Water Vapor Project (NVAP) provides a dataset containing global water vapor values in three layers and is produced by combining balloon-borne and satellite-based measurements (Randel et al 1996, Vonder Haar et al 1999). In this study, NVAP data are used as *a priori* data for the optimal estimation retrieval described in Chapter 3. However, the NVAP dataset only exists for 1988-1997. The HIRS/2 and ACARS data used are from 1999. For this study, 1989 was chosen (arbitrarily) as the year to provide NVAP *a priori* data. This should not affect the results, because the function of *a priori* data is to merely guide the retrieval, not to give the final answer.

The NVAP dataset was produced with 1° spatial resolution in three atmospheric layers: 1000-700 hPa, 700-500 hPa, and 500-300 hPa (1 hecto-Pascal equals 1 millibar). The input for the final product was a combination of radiosondes (mostly over land), TIROS Operational Vertical Sounder (only in cloud-free areas), and Special Sensor Microwave/Imager (only over ocean) measurements. Examples of the data are shown in Figures 2.9 – 2.11.

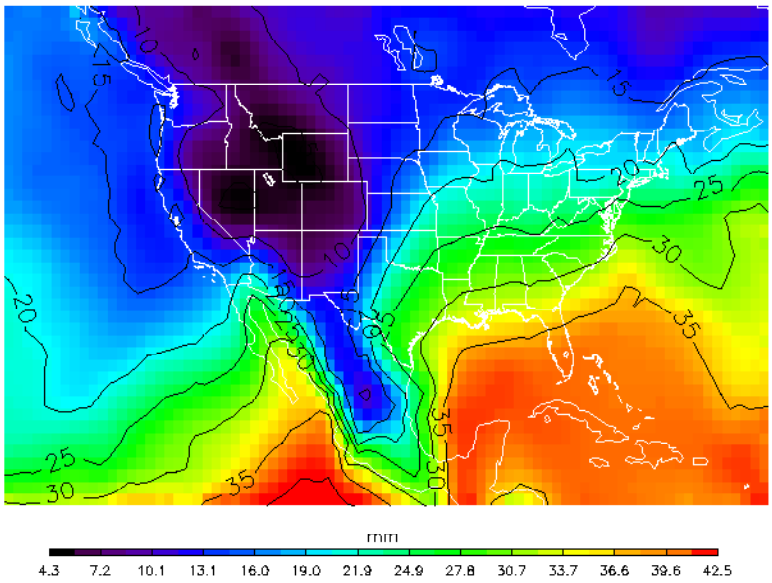

Fig. 2.9 Precipitable water in the 1000-700 hPa layer in August 1989 from the NVAP dataset.

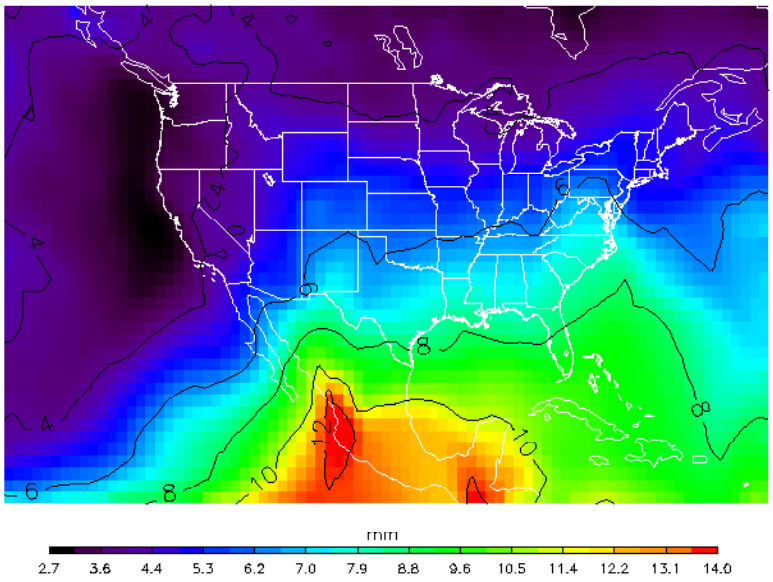

Fig. 2.10 Precipitable water in the 700-500 hPa layer in August 1989 from the NVAP dataset.

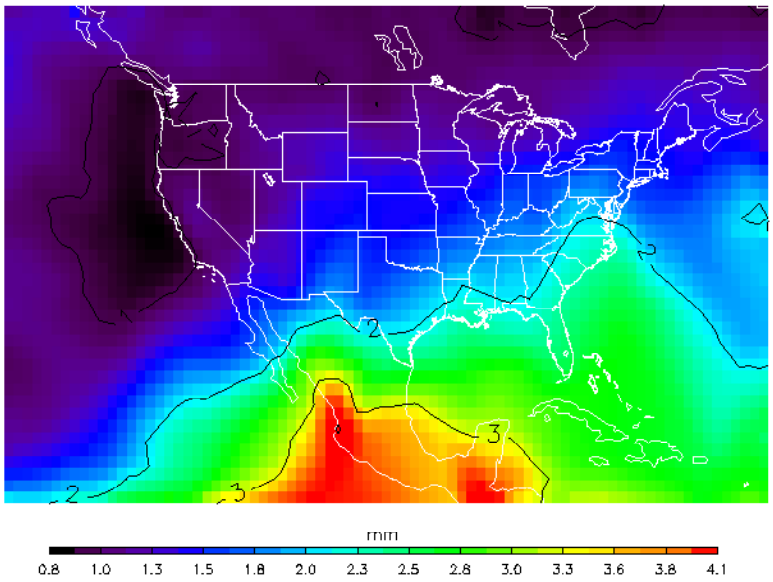

Fig. 2.11 Precipitable water in the 500-300 hPa layer in August 1989 from the NVAP dataset.

2.4 Aircraft Communications Addressing and Reporting System (ACARS)

The Aircraft Communications Addressing and Reporting System (ACARS) has been in operation for over twenty years. However, routine commercial aircraft measurements

of moisture parameters have only been made for the past five years. This new and growing dataset must be used, for it holds valuable information about the water vapor content.

This revolution in temporal and spatial resolution of water vapor measurements is called the Water Vapor Sensing System (WVSS). The instrument responsible for making the measurements is the Vaisala thin-film capacitor (model HMM30D). As shown in Figure 2.12, the instrument is housed inside a larger probe, and the combined package is only eight inches long, making it very easy to place on commercial aircraft (three inches on the outside of the plane, five inches on the inside). During August 1999, there were six units in operation, all on United Parcel Service (UPS) planes; currently there are twenty (Fleming 2001a).

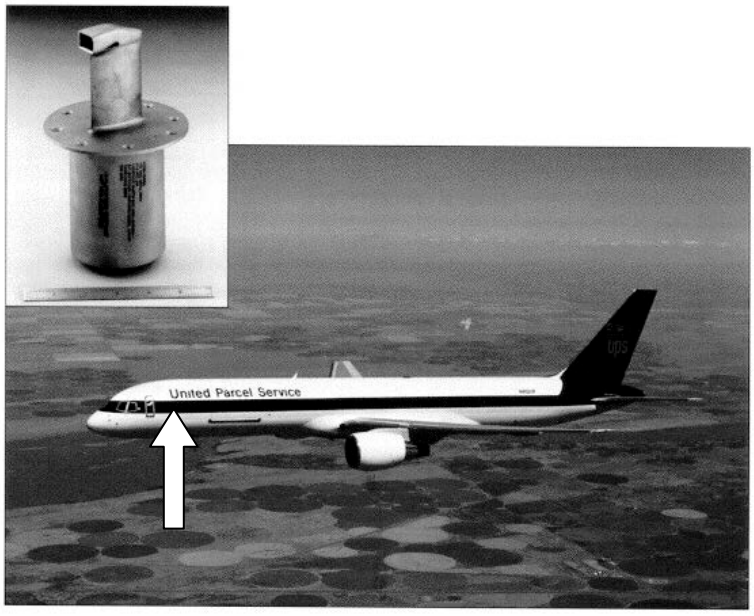

Fig. 2.12 A United Parcel Service B-757 jet carrying the WVSS instrument (inset) (Fleming and Braune 2000).

In the near future, there are plans to install a total of 30 units on UPS planes and 14-18 units on American Airlines planes (Fleming 2001b). This original unit is now called the

WVSS-I. The WVSS-II (Second-Generation Water Vapor Sensing System) will be available as a common off-the-shelf product in 2002.

The instrument directly measures relative humidity and this value is then converted to mixing ratio using the relation:

$$w = \frac{0.62197(RH_{probe})(e_{s,probe})}{100(P_{probe}) - (RH_{probe})(e_{s,probe})}, \tag{2.1}$$

where w is the mixing ratio, RH_{probe} is the relative humidity measured by the probe, $e_{s,probe}$ is the saturation vapor pressure measured by the probe (obtained from RH_{probe} and T_{probe}), and P_{probe} is the dynamic pressure in the probe (according to $P_{probe}=P_{ambient}\ (1+0.2M^2)^{5/3}$ where M is the Mach Number) (Fleming and Braune 2000).

For this study, data from the internet (nearly real-time) had approximately a 5% error in mixing ratio measurements. Dewpoint data from the same source were correct (Fleming and Braune 2000). To convert dewpoint to mixing ratio, the environmental pressure and the water vapor pressure must be calculated. The air pressure varies with altitude according to:

$$p = p_{0,1}\left(\frac{T_1}{T_1 + \Gamma(z - z_{0,1})}\right)^{\frac{gM}{R\Gamma}} \quad \text{for } 0<z<11 \text{ km} \tag{2.2}$$

where p is the air pressure, $p_{0,1}$ is the standard pressure at 0 km (1013.25 hPa), T_1 is the standard temperature at 0 km (288.15 K), Γ is the standard saturated adiabatic lapse rate (-6.5 K km^{-1}), z is the altitude at which the pressure is being calculated, $z_{0,1}$ is the base of the first layer (0 km), g is the gravitational acceleration (9.80665 m s^{-2}), M is the mean molecular mass (28.9644 kg kmol^{-1}), and R is the gas constant (8.31432 N m kmol^{-1} K^{-1}). Likewise,

$$p = p_{0,2} e^{\frac{-gM(z-z_{0,2})}{RT_2}} \quad \text{for } 11<z<85 \text{ km} \tag{2.3}$$

where p is the air temperature, $p_{0,2}$ is the standard pressure at 11 km (226.32 hPa), T_2 is the standard temperature at 11 km (216.65 K), z is the altitude at which the pressure is being calculated, $z_{0,2}$ is the base of the second layer (11 km), and g, M, and R are the same as in Equation 2.3 (NOAA 1976).

Then, find the contribution of water vapor to the total pressure from:

$$T_d = \frac{237.3 \ln\left(\frac{e_{vp}}{6.1078}\right)}{17.27 - \ln\left(\frac{e_{vp}}{6.1078}\right)}. \tag{2.4}$$

where e_{vp} is the vapor pressure and T_d is the dewpoint. Solving for e_{vp} yields:

$$e_{vp} = 6.1078 e^{\frac{17.27 T_d}{237.3 + T_d}} \tag{2.5}$$

The other constants in the equation are empirical. Finally, the mixing ratio is calculated according to the equation:

$$w = \frac{0.622 e_{vp}}{p - e_{vp}} \tag{2.6}$$

where w is the mixing ratio, e_{vp} is the vapor pressure, and p is the air pressure (Wallace and Hobbs 1977).

The temporal resolution of the dataset is phenomenal. Measurements are taken every 0.25 seconds (4 Hz), then averaged to one-second values. However, the data is not reported that frequently. Reports are customized to provide the highest resolution where it is needed the most; namely, in the vertical. During ascent, observations are reported every six seconds for the first 90 seconds of the flight, then every twenty seconds until an altitude of 6.1 km (20,000 feet) is reached. At flight level, observations

are made every 180 seconds. Finally, during descent, observations are made every thirty seconds once the plane is below 6.1 km (20,000 feet). This produces an approximate spatial resolution of 100 meters (330 feet) in the vertical during ascent, 53 kilometers (33 miles) in the horizontal *en route*, and 500 meters (1640 feet) in the vertical during descent (Fleming 1996).

Because of the high resolution, it is very attractive to operational modelers, such as those running the RUC (Rapid-Update Cycle), MM5 (Fifth Generation Mesoscale Model), or even the ECMWF (European Centre for Medium Range Weather Forecasts)(Benjamin et al 1995, Wagoner 2000, Lorenc et al 1996). These measurements are used in conjunction with the common balloon-borne radiosondes released every twelve hours from select sites across the world.

However, at the time this study was conducted, moisture measurements were still not commonplace. Since the United Parcel Service is based out of Louisville, Kentucky, that will be the area of focus, because that is where there are enough measurements to compile frequent, reliable soundings. Hopefully in the near future, all major airports will serve as hubs of reliable water vapor data.

The following figures demonstrate the spatial resolution of the ACARS and WVSS data. Each plot shows a full 24 hours of data, and each point represents a discrete aircraft measurement. Notice the relative sparseness of the mixing ratio data as compared to the more standard temperature data. There are approximately fifty times as many temperature measurements as there are mixing ratio measurements on the same day over the same region. The reason for this is simply the novelty of it; once the technology becomes more widespread, that ratio should decrease significantly.

There is an effort in Germany called MOZAIC (Measurement of Ozone and Water Vapor by Airbus In-Service Aircraft) to make water vapor measurements via commercial aircraft as well. There are currently five A340 aircraft equipped with a humidity sensing

device (Aerodata AD-FS2). MOZAIC flights are concentrated in central Europe, but reach all corners of the globe, much like their American counterpart, ACARS (Marenco 1998, Newell 2000, Kley 2001).

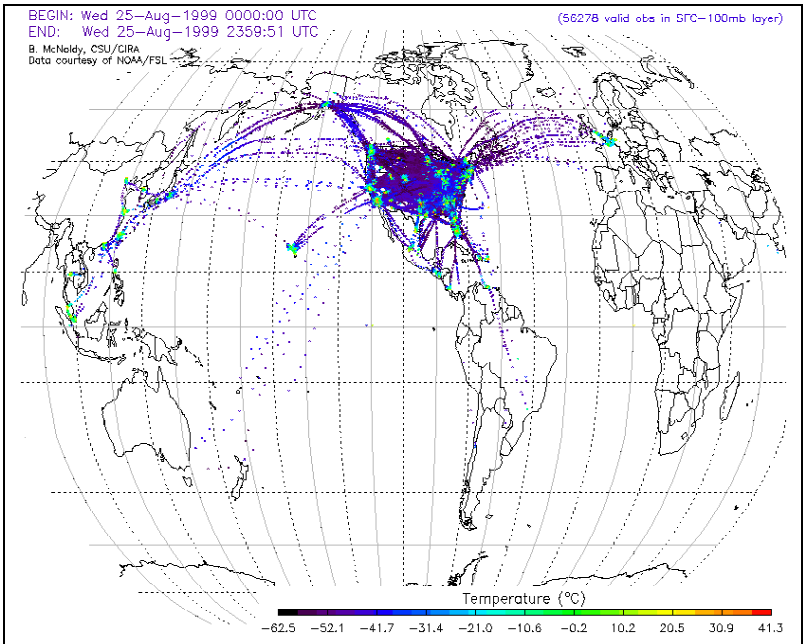

Fig. 2.13 All temperature measurements made by ACARS on August 25, 1999. There are 56,278 data points between the surface and 100 hPa.

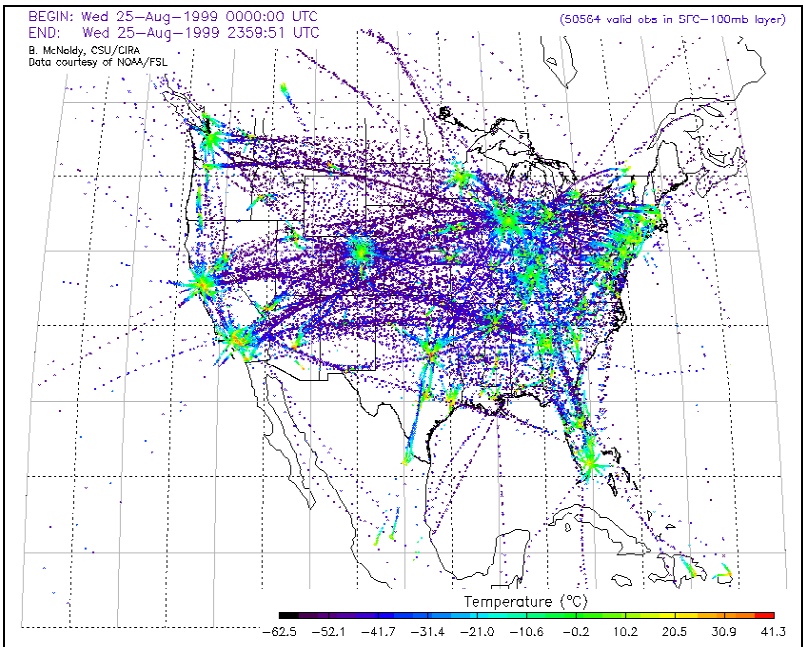

Fig. 2.14 All temperature measurements made by ACARS on August 25, 1999 over the United States. There are 50,564 data points between the surface and 100 hPa.

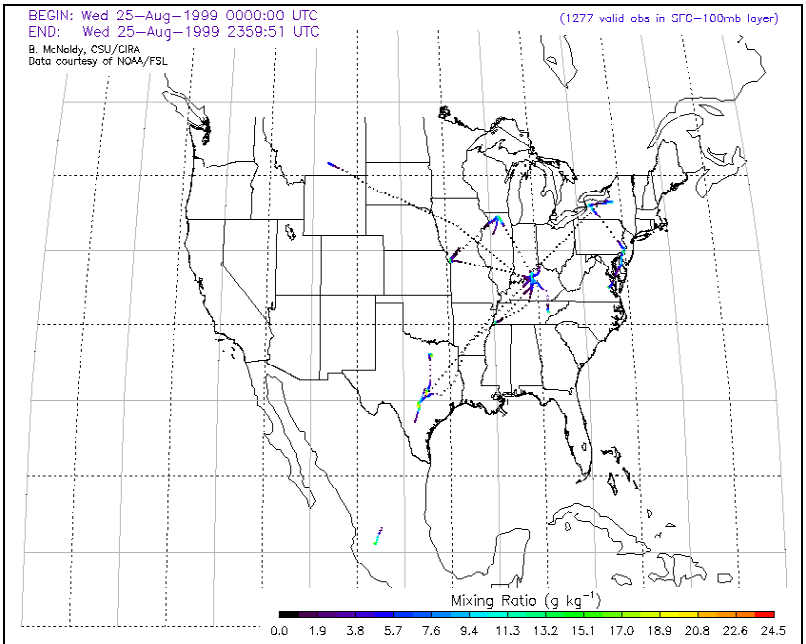

Fig. 2.15 All mixing ratio measurements made by WVSS on August 25, 1999 over the United States. There are 1,277 data points between the surface and 100 hPa.

3. Water Vapor Retrieval

The basis behind retrieval theory is the derivation of atmospheric parameters from measured radiation at the top of the atmosphere (Rodgers 1976). This is called the Inverse Problem. An analogy presented by Stephens (1994) is that of dragon tracks. It is fairly easy to infer what the tracks would look like if one is familiar with the dragon; however, it is much more difficult to deduce what the dragon looks like by looking only at its tracks. In fact, different people may deduce very diverse answers from the same set of tracks. This non-uniqueness dilemma has plagued the satellite-based remote sensing community from the beginning.

3.1 The Inversion and Estimation Problems

3.1.1 Inversion Problem

The inversion problem is one that would seem simple to solve mathematically, but the dependencies of one or more of the variables on many other variables makes it extremely challenging. For example, if $y=f(x)$, then $x=g(y)$. However, if the function f is complicated (containing unknown information about other variables), that simple equation becomes an immense problem to solve. In the case of atmospheric remote sensing, the equation may look something like $I=f(a,b,c,d,e,f)$, where I is the radiation measured by the satellite, and a, b, c, d, e, and f are variables describing the atmospheric state. Suppose one is interested in retrieving d from that equation… $d=g(a,b,c,e,f,I)$, but a, b, c, e, and f may not be known exactly. To arrive at the most likely solution, *a priori* data is required. In this simple example, *a priori* information might mean substituting

known constants for the unknown variables, making the problem much easier to solve directly.

Rodgers (1976) summarized the inverse problem as "the matter of inverting a known equation which expresses radiation as a function of the atmospheric state, so as to express the atmospheric state in terms of radiation". Specific to this study is the problem of inverting a radiative transfer equation in terms of the absorption and emission properties of various gases to get the properties of water vapor as a function of radiation and the properties of other atmospheric gases.

3.1.2 Estimation Problem

Having described the ill-posed inversion problem in the previous section, one can see the need for Estimation Theory (ET). ET attempts to eliminate the ambiguities created by inversion techniques. Basically, using the previous example, ET would give the most likely value for d, given prescribed values for a, b, c, e, and f. Note the phrase "most likely"; ET is not capable of providing a single absolutely correct solution. The Estimation Problem (EP) is "to find the appropriate criteria which determine the best solution from all the possible ones which are consistent with the observations" (Rodgers 1976). Part of the EP is choosing the type and influence of *a priori* data. *A priori* data are "virtual measurements" and are used to guide and bound the inversion process, allowing the inversion to arrive at the most likely solution (Rodgers 1976). In this study, the radiances come from HIRS/2. Those observed radiances are related in some non-unique way to the amount and distribution of water vapor. To arrive at the most likely solution, climatological water vapor (NVAP) data is used as *a priori* to constrain the model.

A very important question relevant to *a priori* is how much weight to place on it. It is used by the forward model (described in the next section), but the magnitude of its

usage must be carefully regulated. If too much weight is placed on it, the forward model will use it exclusively and the measured radiances from the satellite will not even enter the forward model. Conversely, if too little weight is placed on it, the forward model will suffer from non-unique solutions and the chances of arriving at the most likely solution will be greatly diminished. Therefore, *a priori* data is something that must be used in moderation and its role in the final product must be understood.

Two very important parameters in the retrieval are the *a priori* error covariance matrix (S_a) and the forward model error covariance matrix (S_y). These matrices directly affect the output of the retrieval and basically represent the allowed error of the *a priori* data from the real profile and the allowed error of the forward model (the amount of freedom given to the retrieval), respectively. In other words, if S_a is very large, the *a priori* data (NVAP in this case) is assumed to be fairly unreliable, placing a lot of trust in the forward model to arrive at the 'correct' solution. Likewise, if S_y is very large, the forward model is assumed to be unreliable, trusting the *a priori* data to accurately portray the 'correct' solution. For this study, the following values were used to create the two matrices:

$$S_a = \begin{cases} (0.8)^2 & along \quad diagonal \\ (S_{zz}S_{z'z'})^2 \exp\left[-\dfrac{(z-z')^2}{1.5}\right] & off \quad diagonal \end{cases} \tag{3.1}$$

$$S_y[1,1] = (0.07y)^2 \tag{3.2a}$$

$$S_y[2,2] = (0.10y)^2 \tag{3.2b}$$

$$S_y[3,3] = (0.12y)^2 \tag{3.2c}$$

where 0.8 represents 80% of the natural logarithm of the mass mixing ratio, z and z' represent two consecutive altitude levels at which the calculation is performed, and 1.5 is the square of the water vapor scale height (in km) used here. The S_y matrix only has values along the diagonal, and they are defined as 7%, 10%, and 12% times the measured radiances from Channel 10 (lower troposphere), 11 (middle troposphere), and 12 (upper troposphere), respectively. These parameters were chosen to closely mimic those set forth in Engelen and Stephens (1999), the study on which this research builds.

3.2 The Optimum Solution

A clear and concise description of the nonlinear optimal estimation water vapor retrieval used in this study can be found in Engelen and Stephens (1999). In a manner similar to the example presented earlier,

$$y = F(x,b) + \varepsilon_y , \tag{3.3}$$

where y is a vector containing the measured radiances from the satellite, F is the forward model, x is the desired water vapor profile, b is a vector of model parameters (constants describing the state of the atmosphere), and ε_y contains the measurement error characteristics. Linearizing Eqn. 3.3 about x and b yields

$$y(\hat{x},\hat{b}) = F(x,b) + \frac{\partial F}{\partial x}(\hat{x} - x) + \frac{\partial F}{\partial b}(\hat{b} - b) + \varepsilon_y . \tag{3.4}$$

This equation allows one to characterize the errors in the retrieval. The $\hat{}$ denotes estimated quantities (different from *a priori*), and the differential terms $\frac{\partial F}{\partial x}$ and $\frac{\partial F}{\partial b}$ describe the sensitivity of y to Δx and Δb, respectively. At this point, the reader is pointed back to Eqns. 1.1 and 1.2 which first introduced W, the weighting function. Here, W is the same as $\frac{\partial F}{\partial x}$.

To show how the retrieved water vapor profile relates to the error covariance matrices mentioned in the previous sections, the following form of $\hat{x}$ will be provided:

$$\hat{x} = x_a + S_a \left(\frac{\partial F}{\partial x}\right)^T S_y^{-1} \{y - F(\hat{x})\}, \tag{3.5}$$

where x_a is the water vapor *a priori* profile, S_a is the *a priori* error covariance, superscript T represents a matrix transposition, and S_y^{-1} is the inverse of the forward model error covariance matrix.

The Inverse Model will now be introduced; this is what actually performs the inversion described in Section 3.1.1. Using the Inverse Model allows the estimated (retrieved) water vapor profile to be extracted from Eqn. 3.4, resulting in an equivalent expression for Eqn. 3.5:

$$\hat{x} = I(y,b) + \frac{\partial I}{\partial y}(\hat{y} - y) + \frac{\partial I}{\partial b}(\hat{b} - b), \tag{3.6}$$

where I is the Inverse Model, $\hat{y}$ is a synthetic radiance produced by the Forward Model, and $\frac{\partial I}{\partial y}$ and $\frac{\partial I}{\partial b}$ describe the sensitivity of $\hat{x}$ to ε_y and Δb, respectively. Then

$$\hat{x} = I(F(x,b) + x_a, \hat{b}, \varepsilon_y) \tag{3.7}$$

which expresses the retrieved profile as a function of x, x_a, b, $\hat{b}$, and ε_y. Linearizing Eqn. 3.7 about x_a and b yields

$$\hat{x} = \left(\frac{\partial I}{\partial y}\frac{\partial F}{\partial x}\right)x + \left(1 - \frac{\partial I}{\partial y}\frac{\partial F}{\partial x}\right)x_a + \left(\frac{\partial I}{\partial y}\frac{\partial F}{\partial b}\right)(\hat{b} - b) + \left(\frac{\partial I}{\partial y}\right)\varepsilon_y. \tag{3.6}$$

This is the final form of the equation that is used to retrieve a water vapor profile from the measured radiances and known model parameters, sensitivities, and *a priori* data

(Engelen and Stephens 1997, Engelen and Stephens 1999, Rodgers 1976, Rodgers 1990).

3.3 Application to TOVS

Applying the retrieval described in the previous section to TOVS HIRS/2 radiances results in Figures 2.5-2.8. The retrieval produces precipitable water values (very closely tied to water vapor content) in four layers of the troposphere: 1000-700 hPa, 700-500 hPa, 500-300 hPa, and 300-200 hPa. The results and validation of this data to other satellite-based measurements are described in detail in Engelen and Stephens (1999), Engelen and Stephens (1998), Berg et al (1999), Smith (1991), and Eyre (1990).

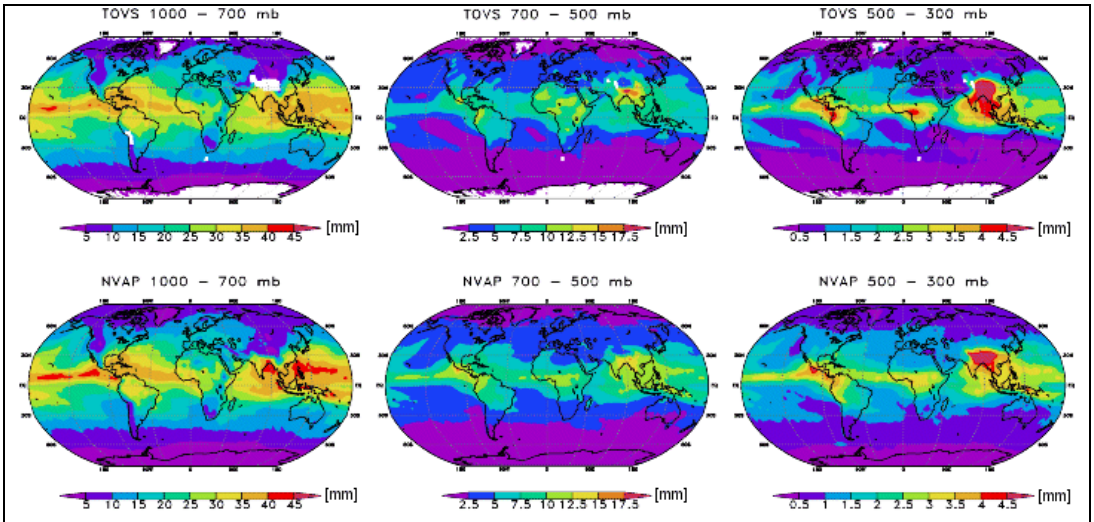

Fig. 3.1 A comparison of TOVS HIRS precipitable water output to that of the *a priori* NVAP data in the lower three layers. TOVS shows very good agreement in both distribution and magnitude with NVAP (Engelen and Stephens 1999).

A brief sensitivity study conducted by Engelen and Stephens (1999) will be presented here. Figure 3.2 shows how the TOVS retrieval performs under varying input. The six graphs are simply a result of choosing six different pressure levels at which to analyze the differences (recall x and $\hat{x}$ are vectors). The most important feature to notice about the graphs is how the peak amplitude of the response function changes

(solid curve); the greater the amplitude, the more sensitive TOVS is to water vapor concentration changes at that level. Notice that the instrument is most sensitive at 1000 hPa and in the 300-350 hPa range and least sensitive in the 700-500 hPa range as well as the extreme upper troposphere at 200 hPa.

The patterns in Figure 3.1 also demonstrate this behavior. In the 1000-700 hPa layer, TOVS underestimated the values by about 10%; in the 700-500 hPa layer, there was strong agreement; and in the 500-300 hPa layer the agreement is also very good. The reason for the differences is the pressure-dependency of *a priori* data: it is highly dependent at the surface to minimally dependent at the higher altitudes. These results were also verified in this study.

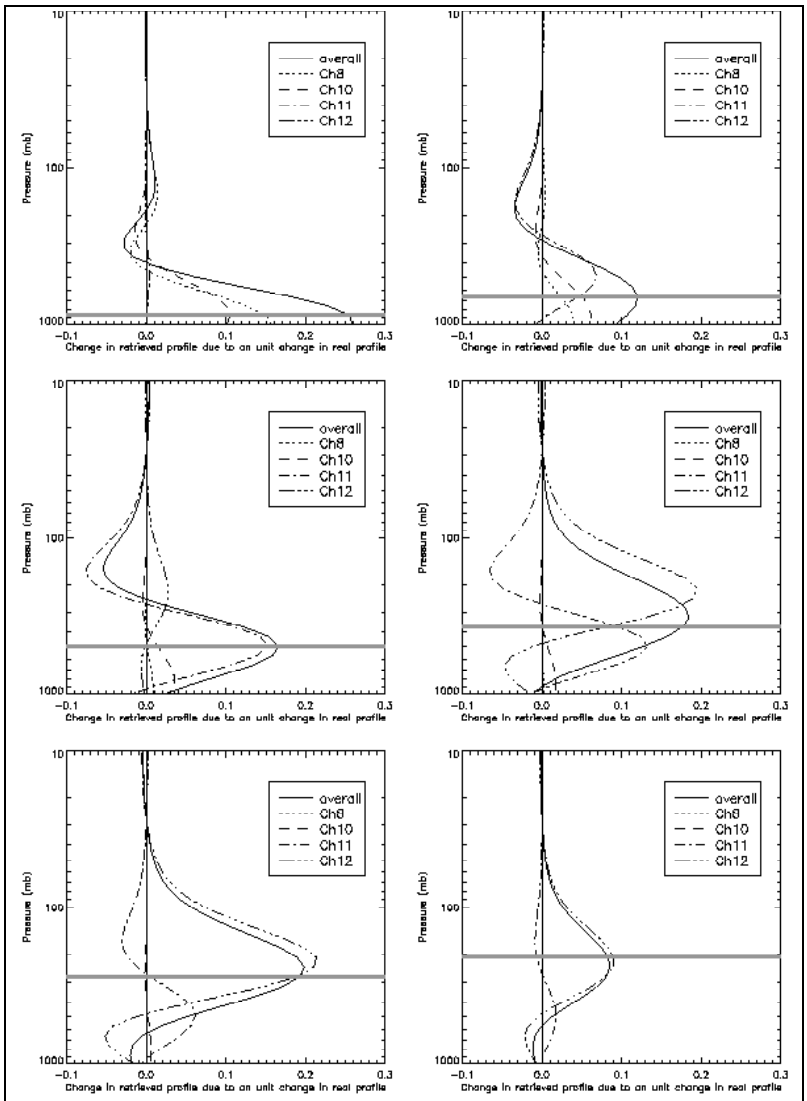

Fig. 3.2 Change of TOVS retrieved water vapor concentration due to a change in the real water vapor concentration for six pressure levels: 1000 hPa, 700 hPa, 500 hPa, 350 hPa, 300 hPa, and 200 hPa (Engelen and Stephens 1999).

4. Validation Method

The word *validation* is defined as “the act of finding or testing the truth of something”. This is a demanding task, and something that is rarely definitive, despite the implication. This study is loosely classified as a validation because a relatively accurate method of measuring water vapor mixing ratio (aircraft) is being compared to a much less accurate method (satellite). Since satellites provide coverage of the global atmosphere, the goal is to test the satellite method for biases or incorrectness so it can be used in conjunction with aircraft measurements without fear of significant errors. The extent of the “validation” is also limited, and the details of the limitations will be discussed in Sections 4.1 and 4.2.

4.1 Constraints and Limitations

4.1.1 Times

As discussed earlier (Section 2.2), the HIRS/2 data were only available for August 1999, so the possible times to perform “validation” studies are already quite limited. Secondly, the HIRS/2 data were cloud-cleared, meaning that any cloudy pixels (a pixel containing a “cloud”) in the raw data were replaced with a known “clear” pixel; therefore, any cloudy days over an area of interest were not of any use in this study because the data were not actually observed (the observed radiances were replaced). The availability of WVSS measurements added a third, larger restriction. Since all WVSS instruments are currently installed on only six UPS jets, the flight pattern of UPS jets becomes critical. Also, as seen in Figure 2.15, the number of mixing ratio

measurements is still low compared to other measured parameters. The result is only eight days of reliable data, all centered over Louisville, Kentucky (38°11'N, 85°44'W). The implications of this will be discussed further in Section 4.2.

The selected days are 01Aug (Julian Day 213), 05Aug (JD 217), 06Aug (JD 218), 20Aug (JD 232), and 25Aug-28Aug (JD 237-240). Figure 4.1 shows an infrared image (11μm) of the study area for each of the case study days; the images are a composite of the GOES 8 and GOES 10 Imager Channel 4 (the two United States operational geosynchronous satellites at the time).

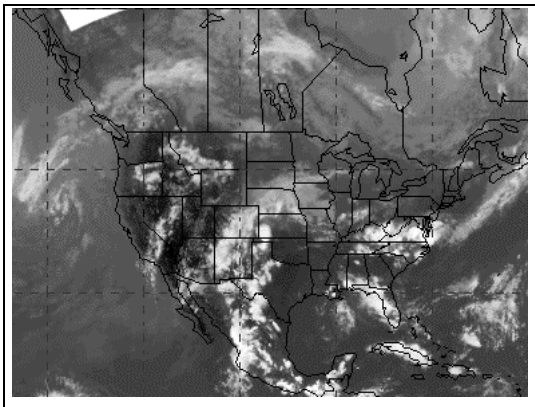

01Aug99 (JD 213), 2345Z

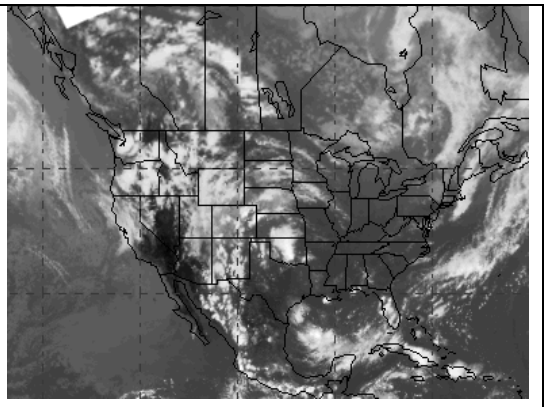

05Aug99 (JD 217), 2345Z

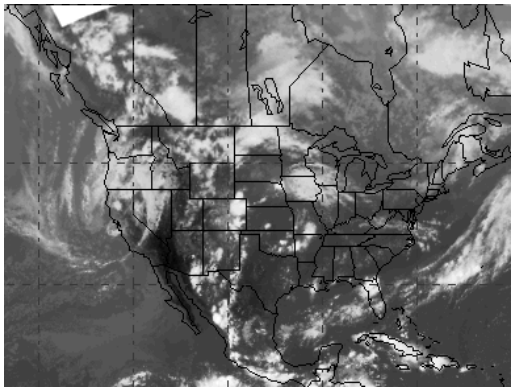

06Aug99 (JD 218), 2345Z

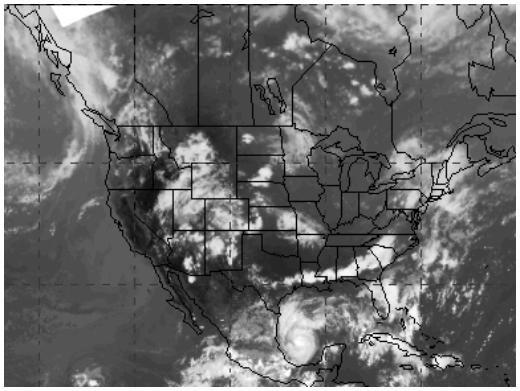

20Aug99 (JD 232), 2345Z

Fig. 4.1 Continued with caption on next page.

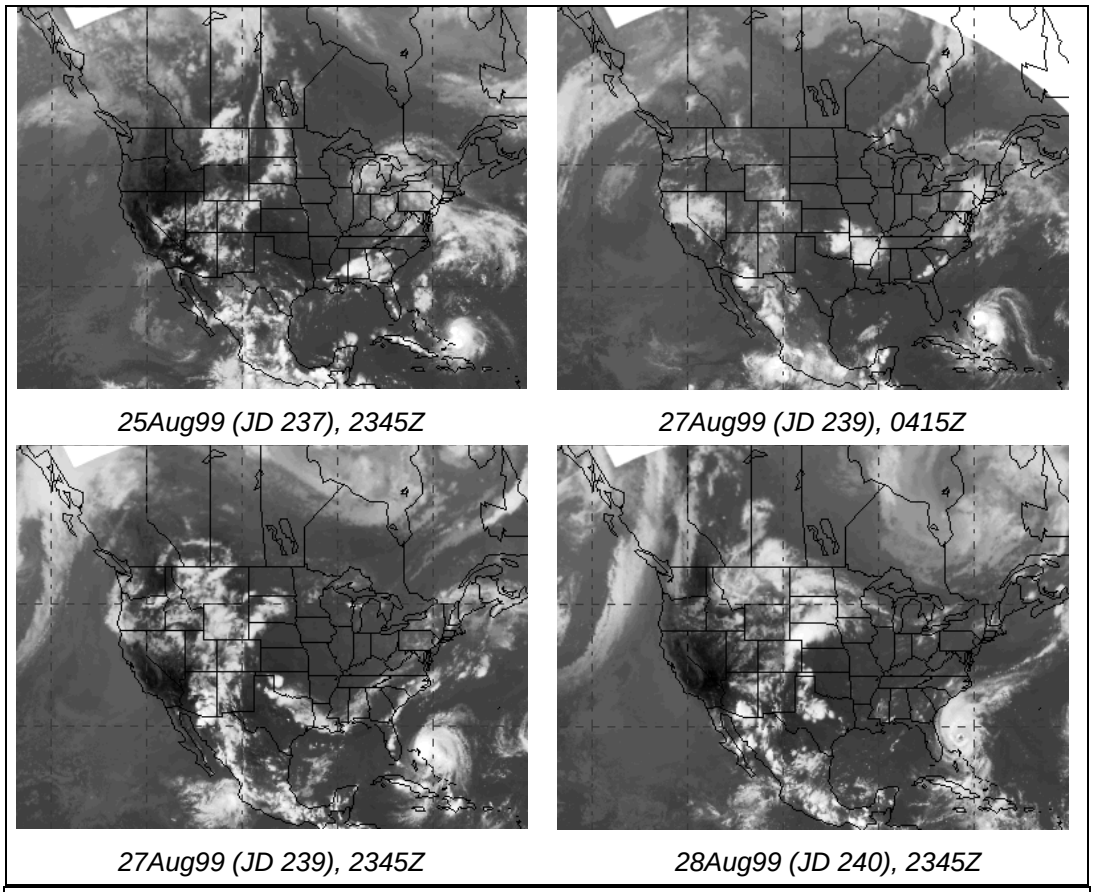

Fig. 4.1 Infrared images for each of the eight case study days. Brighter colors indicate colder temperatures. (Images courtesy of Unisys).

4.1.2 Locations

There are several factors that went into deciding upon the location to be used for the study. The HIRS/2 data were not restrictive at all; there is global coverage, and the only requirement would be for no clouds on the day of interest over the study area. The aircraft data coverage is the major limiting factor. Not only do the UPS jets fly primarily over the continental United States (Figure 2.13), but the water vapor measurements are made only over a few major airports in the continental United States. In fact, there are so few measurements at the time of this study that to make a reliable composite sounding, only the most frequently visited airports are useable. The best site (most frequently visited) found is Louisville, Kentucky, United Parcel Service headquarters.

Other cities/airports such as Miami, Atlanta, New York City, Chicago, Omaha, Dallas, Denver, Salt Lake City, San Francisco, Los Angeles, or Seattle may have ample flights on a given day, but typically there are many fewer or none at all on subsequent days from that same airport, making a comparison study nearly impossible.

In time, as the WVSS system grows, this will not be a problem and the "validation" performed in this study for Louisville will be reproducible for any of the other major airports. A key limitation is that only a certain latitude and climate region is sampled here; it would be beneficial to examine higher and lower latitudes, coastal and mountain sites, *et cetera*.

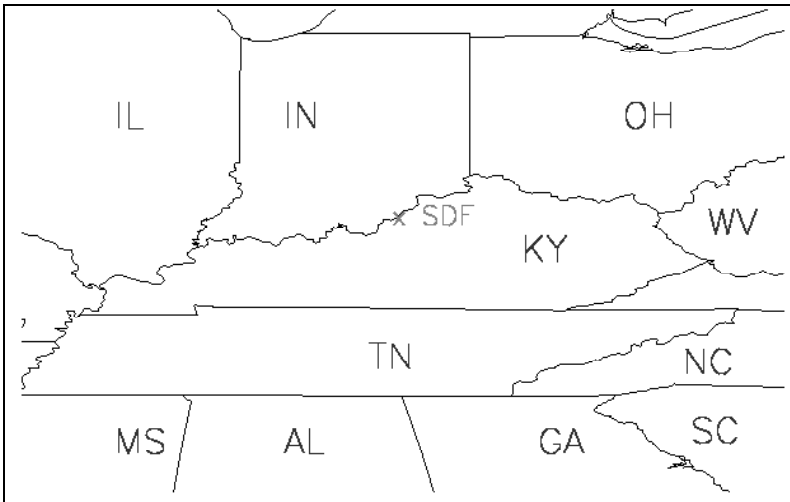

Fig. 4.2 Map showing the location of Louisville, Kentucky (SDF) and neighboring states.

For each case study day, a vertical profile, or sounding, of precipitable water, was produced from the aircraft data, satellite data, and *a priori* data. For the aircraft data, all flights into and out of Louisville on a given day were tracked and any measurement made within 1.5° of the airport (approximately 145 km radius) was counted as a data point (a sounding is ideally vertical, but aircraft cannot take off or land vertically, so some space is needed to account for that). All of the points were then averaged in 100 hPa layers and converted from water vapor mixing ratio to precipitable water. Aircraft

measurements sometimes only extended up to 450 hPa (6.4 km), and other times as high as 200 hPa (11.8 km). For the satellite and *a priori* data, the exact location of Louisville was used to find the precipitable water value in each of the four layers described in Section 2.2.

The WVSS data points needed to be converted from point water vapor mixing ratio measurements to precipitable water in a layer. Precipitable water is typically measured in millimeters (or centimeters), while mixing ratio is typically measured in g kg^{-1}. The conversion used here is

$$PW = \frac{1}{g}\int_{p_1}^{p_2} r\,dp\,. \tag{4.1}$$

Computationally, Eqn 5.1 can be written as

$$PW = \frac{r\Delta p}{10g}, \tag{4.2}$$

where PW is precipitable water in millimeters, r is water vapor mixing ratio in g kg^{-1}, Δp is the thickness of the atmospheric layer in millibars, and g is the Earth's gravitational acceleration in m s^{-2}.

4.2 Summary of Scope and Limiting Factors

The primary constraints and limitations have been discussed already, but a summary will be provided here. First, the dates of the case studies are limited to August 1999 by data availability. Further limitations arise due to aircraft water vapor availability (when were there reliable soundings over a given airport). Finally, once the first two criteria were met, the day needed to be checked for cloudiness over the site of interest.

The union of all of these constraints resulted in eight days of vertical soundings over Louisville, Kentucky. Clearly, this study is extremely limited in scope, but it is also a *preliminary* assessment due largely to the infancy of the WVSS.

5 Results

This chapter will illustrate the comparisons of the vertical profile of precipitable water over Louisville, Kentucky for selected case study days. In all cases, three profiles are shown, one from the aircraft, one from the satellite-based water vapor retrieval algorithm, and one from the *a priori* data to show how the others compare to climatology.

5.1 Vertical Profile Comparisons

As mentioned earlier, the results presented here are preliminary; there are few other studies against which they can be compared. The case studies were selected by the rules outlined in Section 4.1.

Each of the plots contains three vertical profiles, or soundings. The first is from the retrieval algorithm performed on the HIRS/2 data. Those data exist at four levels, so there are only four points along the curve (the points are plotted at the logarithmic half-way mark in the layer; i.e., 245 hPa is halfway between 200 and 300 hPa, 387 hPa is half way between 300 and 500 hPa, etc).

The second profile is from aircraft measurements using the WVSS. Due to the continuum of measurements, it was necessary to create a layer average to mimic the resolution of the satellite data. The discrete mixing ratio measurements were converted to a value of precipitable water in a layer using an integration technique described in Section 4.1.

The third and final profile is from the NVAP climatology values for August 1989. A monthly average in almost any year would be fairly representative of that month's climatology; plotting this along with the other two curves allows one to see 1) how

closely the retrieved sounding follows it (recall the NVAP data were *a priori* data for the retrieval) and 2) how similar that particular day in August 1999 was to climatology.

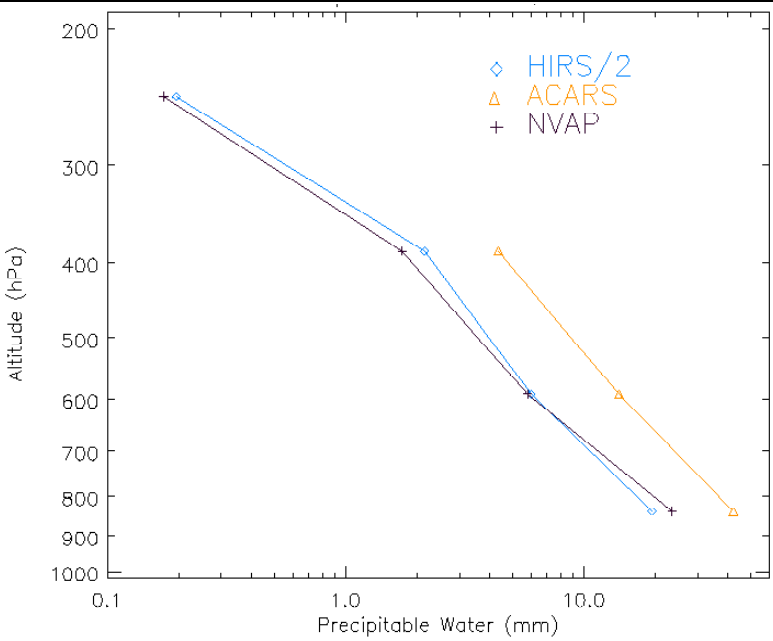

Fig. 5.1 Precipitable water profiles over Louisville, Kentucky (SDF) on August 1, 1999.

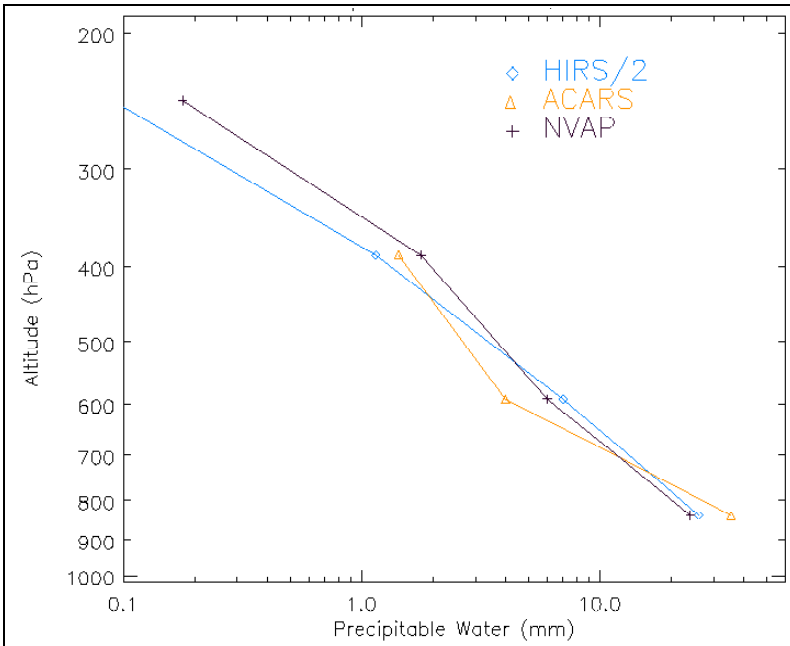

Fig. 5.2 Precipitable water profiles over Louisville, Kentucky (SDF) on August 5, 1999.

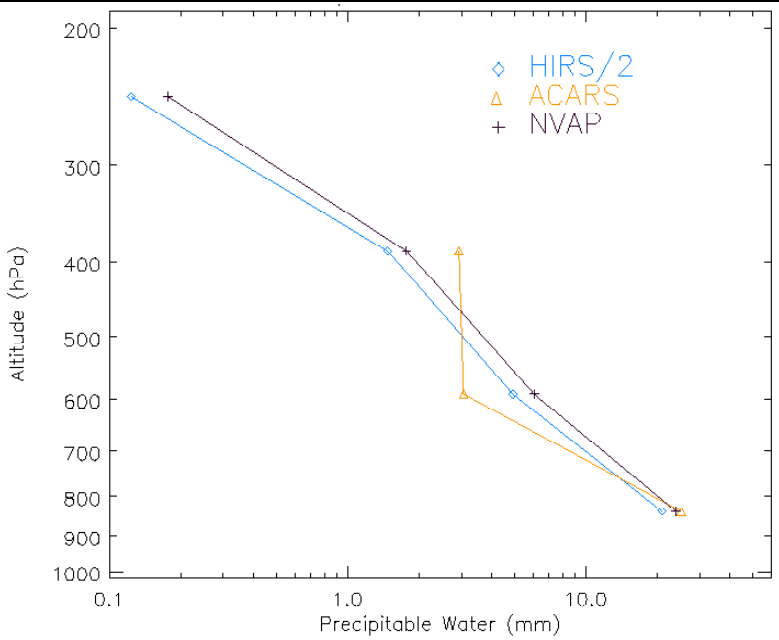

Fig. 5.3 Precipitable water profiles over Louisville, Kentucky (SDF) on August 6, 1999.

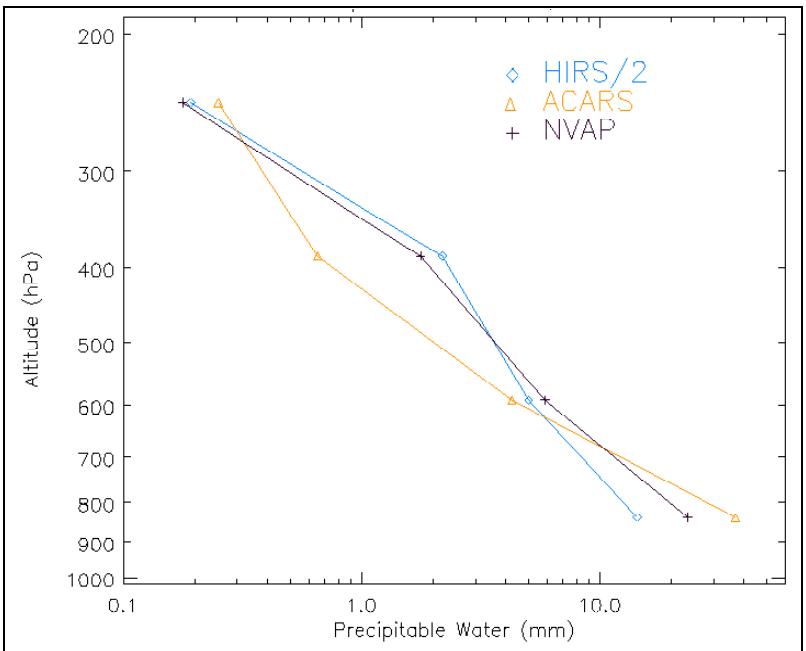

Fig. 5.4 Precipitable water profiles over Louisville, Kentucky (SDF) on August 20, 1999.

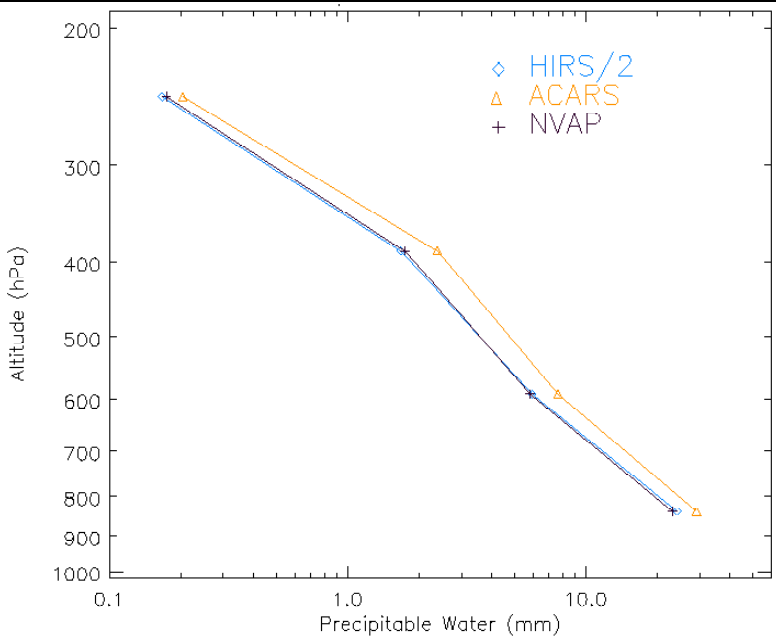

Fig. 5.5 Precipitable water profiles over Louisville, Kentucky (SDF) on August 25, 1999.

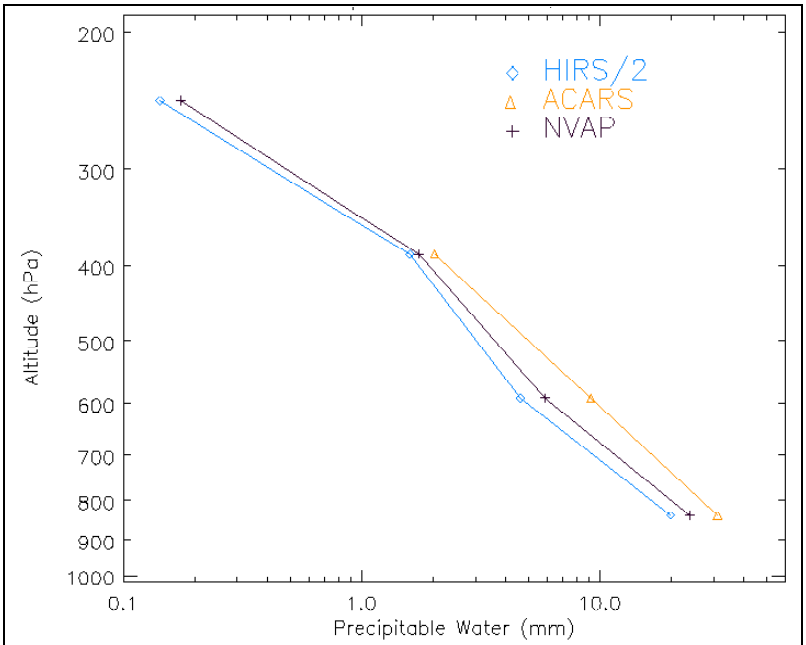

Fig. 5.6 Precipitable water profiles over Louisville, Kentucky (SDF) on August 26, 1999.

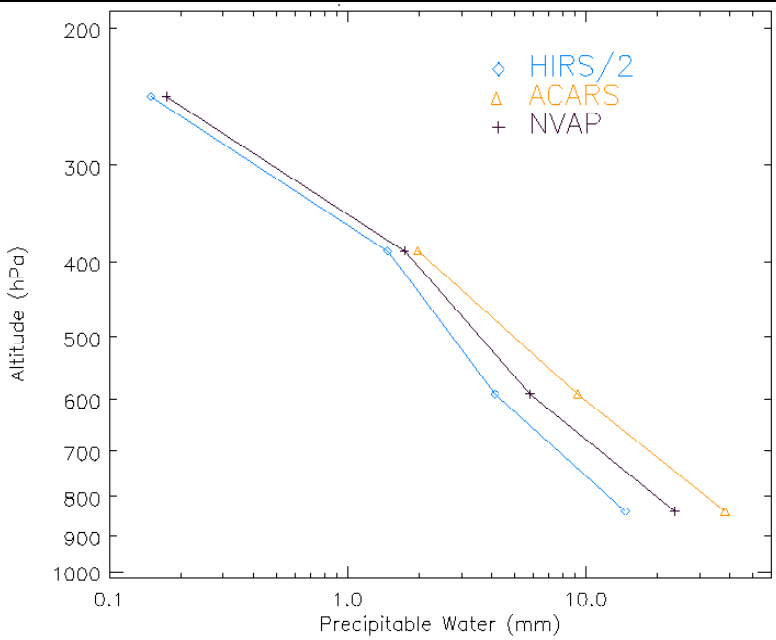

Fig. 5.7 Precipitable water profiles over Louisville, Kentucky (SDF) on August 27, 1999.

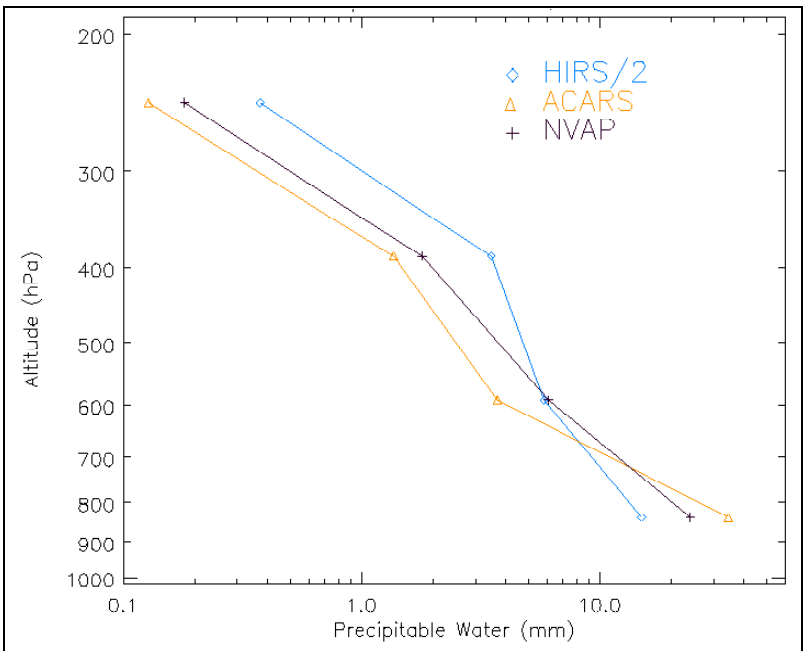

Fig. 5.8 Precipitable water profiles over Louisville, Kentucky (SDF) on August 28, 1999.

The eight cases presented here demonstrate similar behaviors. Occasionally, all three curves are very comparable, but more commonly, ACARS (WVSS) is the wettest; implying that that the HIRS/2 retrieved profiles are generally dry-biased. Based on that

alone, one can infer that August 1999 was a wetter month (at least in Kentucky) than was August 1989.

Before describing each case individually, it is important to understand how to correctly interpret the HIRS/2 curves; it is a special case because it is a retrieved quantity, not measured or observed directly. The retrieval relies heavily on *a priori* data at the surface, less heavily in the middle, and only lightly in the upper levels. That is, the instrument sensitivity (via weighting functions) increases with altitude, so, the low levels are characterized by low sensitivity and high dependence on *a priori*; the mid levels are characterized by moderate sensitivity and moderate dependence on *a priori*; and the upper levels are characterized by high sensitivity and low dependence on *a priori* (Engelen and Stephens 1999). In essence, the closer the HIRS/2 line is to the ACARS line, the better the retrieval. This is especially true in the upper levels, where the retrieval algorithm depends less on the NVAP data as guidance and more on its own "skill". A brief description of each case will be provided in the following paragraphs (coinciding with Figures 5.1 - 5.8), to add some insight to the results. Errors and/or biases will be discussed in Section 5.2.

One of the poorer cases is 01Aug. In all three levels where there is aircraft data available, the HIRS/2 curve is significantly drier. One can also see that the retrieved curve did not deviate from the *a priori* curve very much. Although not very clear in this case, it is the first of four cases in which the retrieved profile oscillates about the *a priori* profile. This may be due to noise in the original HIRS/2 radiances being amplified by the retrieval algorithm. This case is also the primary suspect for possible cloud contamination or incorrect cloud-clearing. The top-left infrared satellite image in Figure 4.1 showed that a large weather system was exiting the Kentucky area on this day, so it is not surprising that the frequent aircraft soundings would measure that copious

moisture, while the satellite may have had one of its passes occur after the system moved through.

Case 2, 05Aug, shows a very different scenario. In this case, the HIRS/2 and the ACARS curves agree rather well, especially in the 1000-700 hPa layer and the 500-300 hPa layer. In the 700-500 hPa layer, ACARS is almost twice as dry as HIRS/2. The uppermost point of the HIRS/2 curve is very dry and is actually just out of the range of the graph. Again, notice how the retrieved profile oscillates about the *a priori* profile.

The 06Aug case is peculiar in that the ACARS curve does not demonstrate the expected linear drop-off on a logarithmic scale. Instead, the second and third layers are very similar in terms of precipitable water, perhaps indicative of the remnants of a major mesoscale convective complex approaching the area, bringing with it significant mid-level moisture. This is the first of three cases where the retrieved profile is consistently drier than the *a priori* profile at all four levels. This bias is most likely caused by the measurement covariance being slightly too high.

Case 4, or 20Aug, is the first case of three in which aircraft data are available up to the 300-200 hPa layer. The retrieved profile once again exhibits an oscillatory behavior, showing skill in the 700-500 hPa and 300-200 hPa layers, but performing poorly in the other layers. Notice that the ACARS value at the lowest layer is nearly three times as high as the HIRS/2 value there.

The 25Aug graph shows a remarkable series of profiles. A key feature is that the HIRS/2 profile does not deviate from the *a priori* profile at all through the entire atmosphere. Secondly, the ACARS profile closely mimics that same pattern, indicating some skill in the retrieval because of the low error through all 800 hPa.

Case 6, 26Aug, is another case where the retrieved profile is consistently drier than the *a priori* profile (though not by much). Although the errors are not large at any of the

three levels, it is interesting to note that the HIRS/2 profile is actually drier than the NVAP profile, while the actual measurement profile is wetter than NVAP.

Likewise, 27Aug exhibits the same features as 26Aug. The only difference in this case is the spread between the HIRS/2 and ACARS curves increases in the lower levels relative to the previous case.

Finally, the 28Aug graph shows that 1) aircraft data reach the 300-200 hPa layer again, and 2) the HIRS/2 profile oscillates about the NVAP profile. As mentioned earlier, that oscillation may be due to noise in the HIRS/2 radiances. If that is the case, it would explain why the retrieval is unable to match the ACARS profile, and instead, incorrectly adjusts beyond the a priori profile at all levels.

5.2 Error Characteristics

5.2.1 Retrieval Parameters

Some retrieval parameters have already been discussed, such as the *a priori* covariance (Eqn 3.1) and the measurement covariance (Eqns 3.2 a-c). Some other parameters will now be discussed to demonstrate how useful and successful the retrieval was.

An initial check to ensure that the retrieval is correctly interpreting the measured radiances is to compare the measured (y) and modeled ($F(x)$) radiances. The percentage difference between those two should be less than (or equal to) the measurement covariance values (S_y), which is shown in Equations 5.1 a-c:

$$\frac{y_{10} - F(x_{10})}{y_{10}} \times 100 \leq 7\% \qquad (\textit{for} \quad \textit{Channel} \quad 10), \tag{5.1a}$$

$$\frac{y_{11} - F(x_{11})}{y_{11}} \times 100 \le 10\% \qquad (\textit{for} \quad \textit{Channel} \quad 11), \tag{5.1b}$$

$$\frac{y_{12} - F(x_{12})}{y_{12}} \times 100 \le 12\% \qquad (\textit{for} \quad \textit{Channel} \quad 12). \tag{5.1c}$$

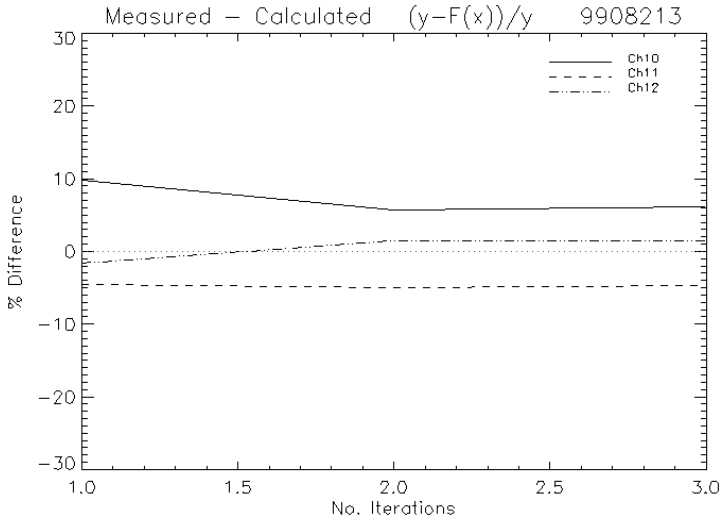

Fig. 5.9 Forward Model performance over Louisville, Kentucky (SDF) on August 1, 1999.

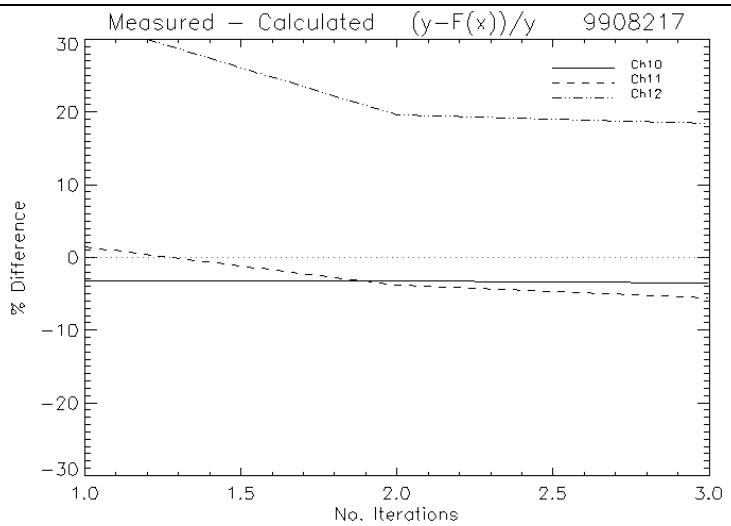

Fig. 5.10 Same as Fig 5.9, but for August 5, 1999.

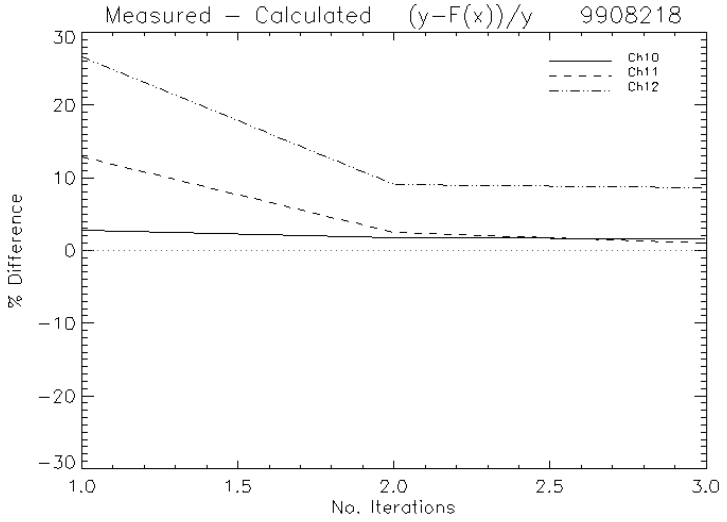

Fig. 5.11 Same as Fig 5.9, but for August 6, 1999.

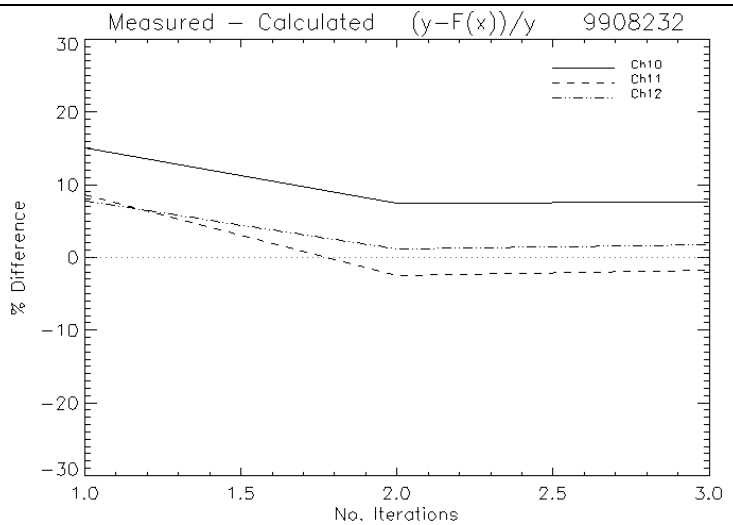

Fig. 5.12 Same as Fig 5.9, but for August 20, 1999.

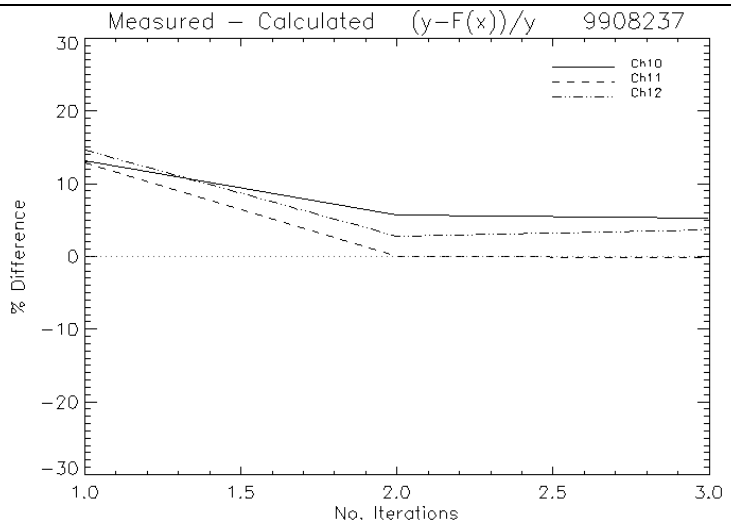

Fig. 5.13 Same as Fig 5.9, but for August 25, 1999.

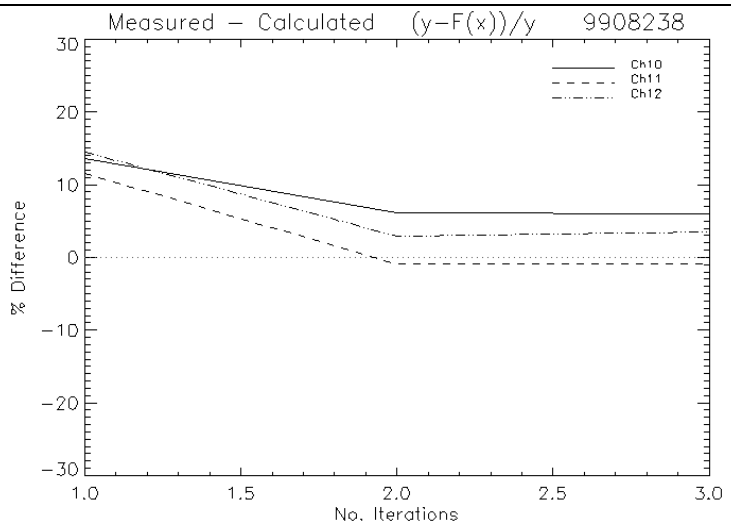

Fig. 5.14 Same as Fig 5.9, but for August 26, 1999.

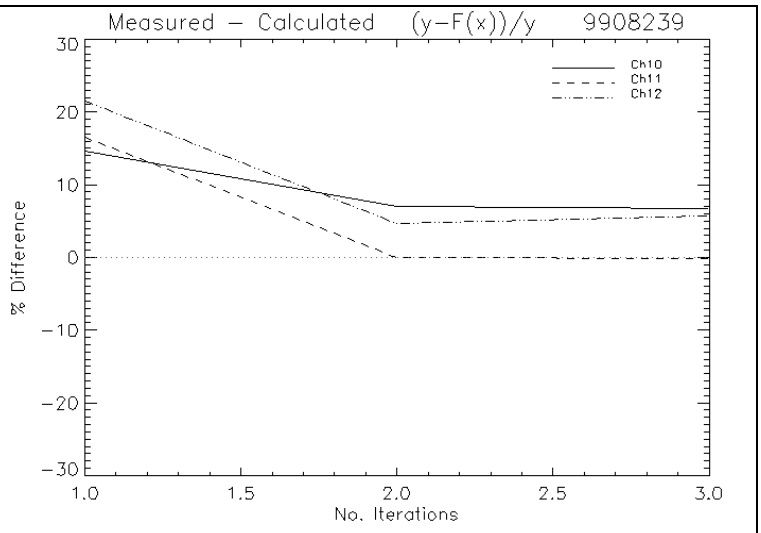

Fig. 5.15 Same as Fig 5.9, but for August 27, 1999.

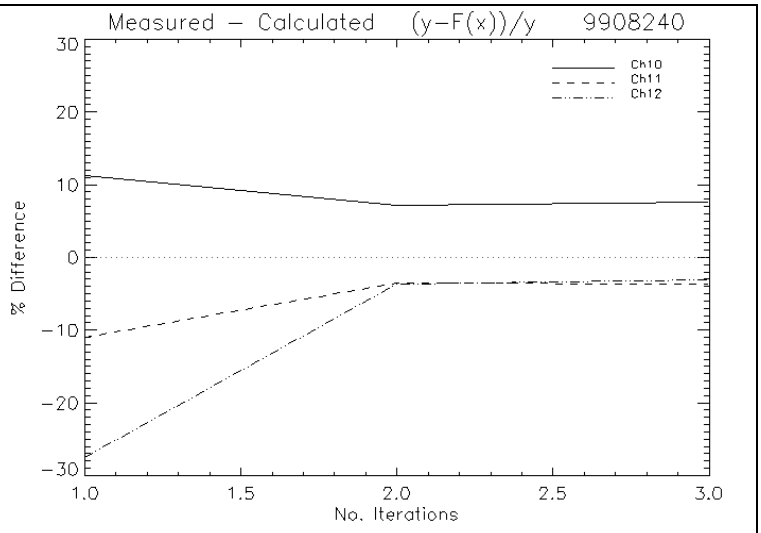

Fig. 5.16 Same as Fig 5.9, but for August 28, 1999.

From these figures, one can see that there are only three instances (out of 24) where the model failed to converge to within the prescribed errors: Channel 12 on 05 Aug, Channel 10 on 20 Aug, and Channel 10 on 28 Aug. The first instance is the most severe, while the latter two are only barely outside the limits. Basically, any case where the model fails to converge for a particular channel, one must be aware that the corresponding retrieved layers (lower troposphere for Ch10, middle troposphere for Ch11, and upper

troposphere for Ch12) may not be making full use of the retrieval, and more from the *a priori* data.

It is instructive to introduce the averaging kernel, A, which is basically the sensitivity of the observing system to deviations in the real water vapor profile and is mathematically described by $\frac{\partial I}{\partial y}\frac{\partial F}{\partial x}$ (found in Eqn 3.6). The averaging kernel can be interpreted as the retrieval's dependence on *a priori* data. For substantial dependence, A will tend toward zero, and conversely, for minimal dependence (ideal measurements), A will tend toward unity (the identity matrix). The columns of this matrix "represent the response of the system to a delta-function change in water vapour at a specified pressure" (Engelen and Stephens 1999). Plots of the averaging kernel are shown in Figures 5.17 – 5.24, corresponding to the eight case study days. Note that the average peak column sum (Σ) lies at the 500 – 700 hPa layer; this is where the retrieval is most sensitive to fluctuations in water vapor concentrations (followed by 300 – 500 hPa, then 700 – 1000 hPa, and finally 200 – 300 hPa).

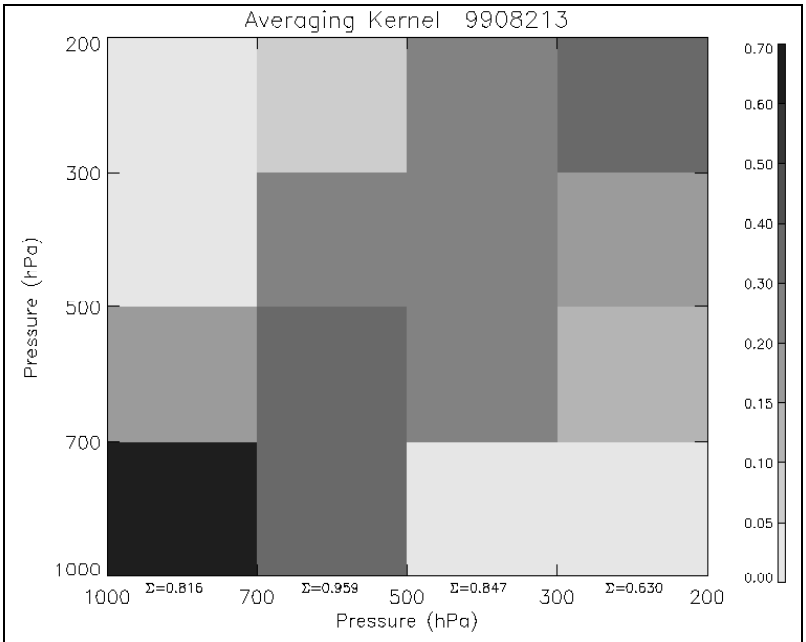

Fig. 5.17 Averaging kernel (A) over Louisville, Kentucky (SDF) on August 1, 1999.

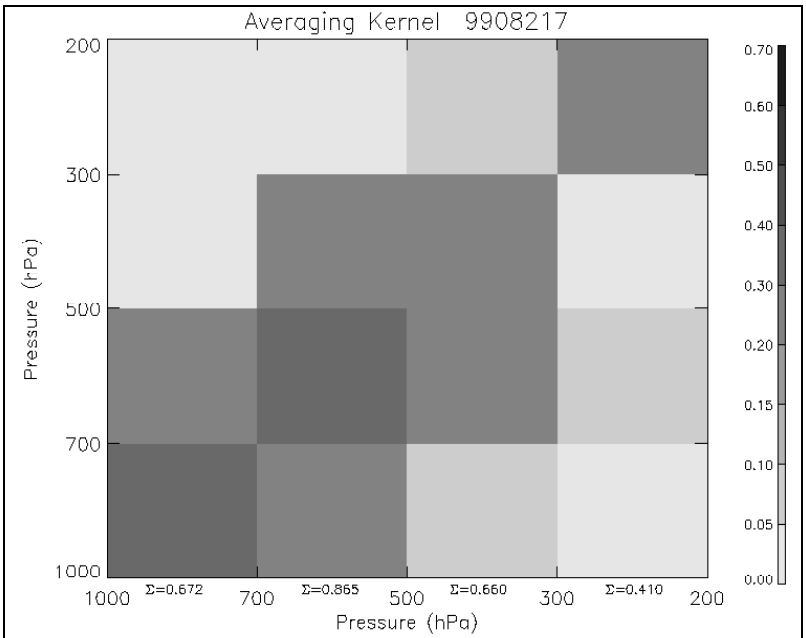

Fig. 5.18 Same as Fig 5.17, but for August 5, 1999.

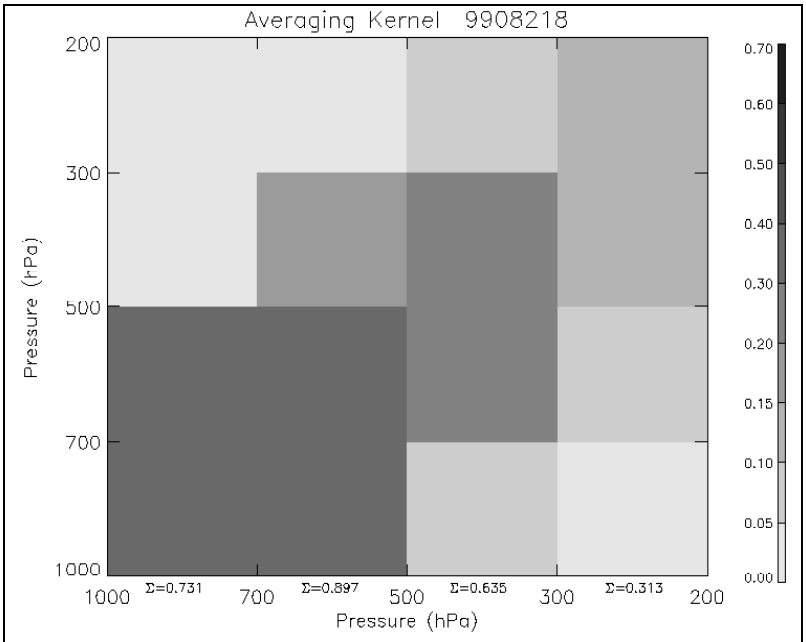

Fig. 5.19 Same as Fig 5.17, but for August 6, 1999.

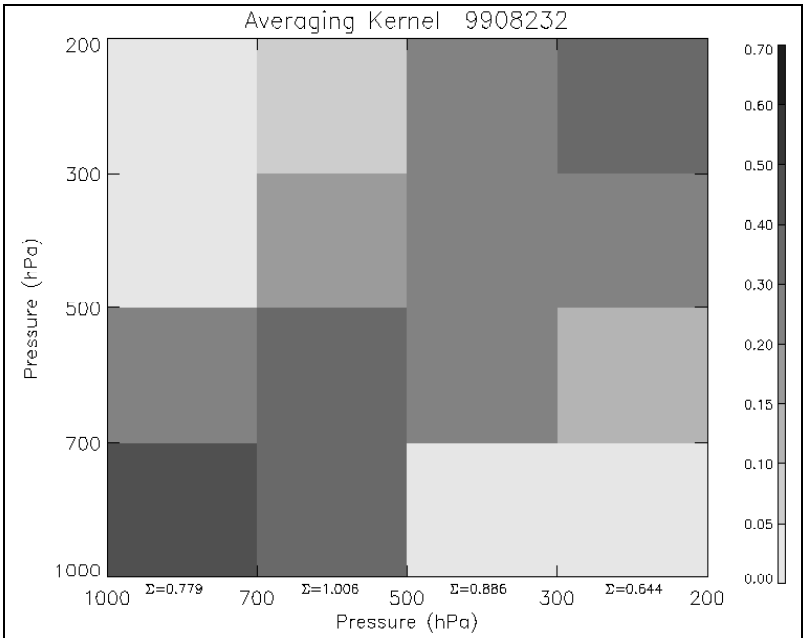

Fig. 5.20 Same as Fig 5.17, but for August 20, 1999.

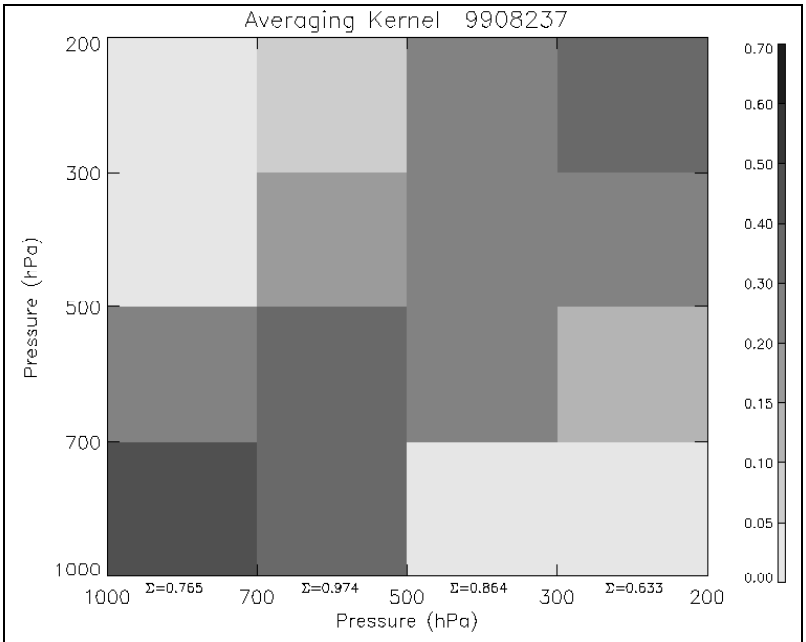

Fig. 5.21 Same as Fig 5.17, but for August 25, 1999.

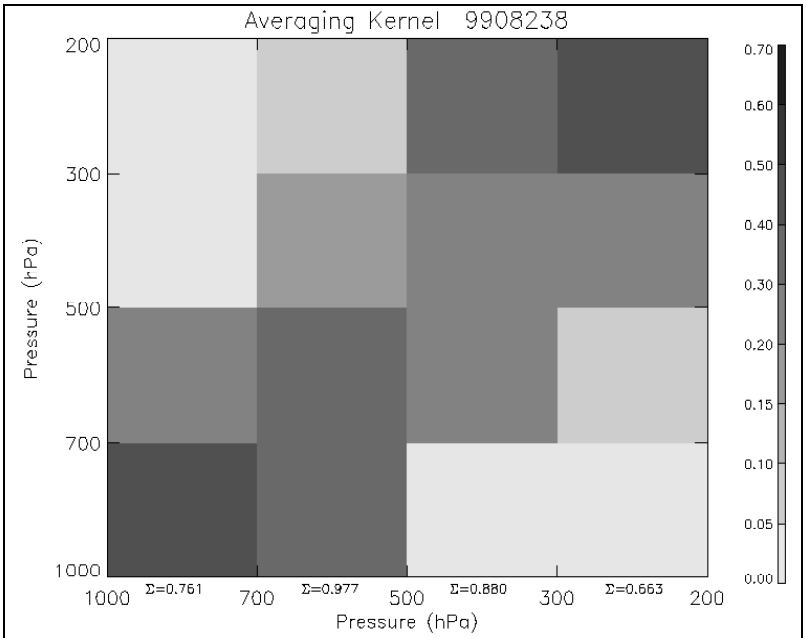

Fig. 5.22 Same as Fig 5.17, but for August 26, 1999.

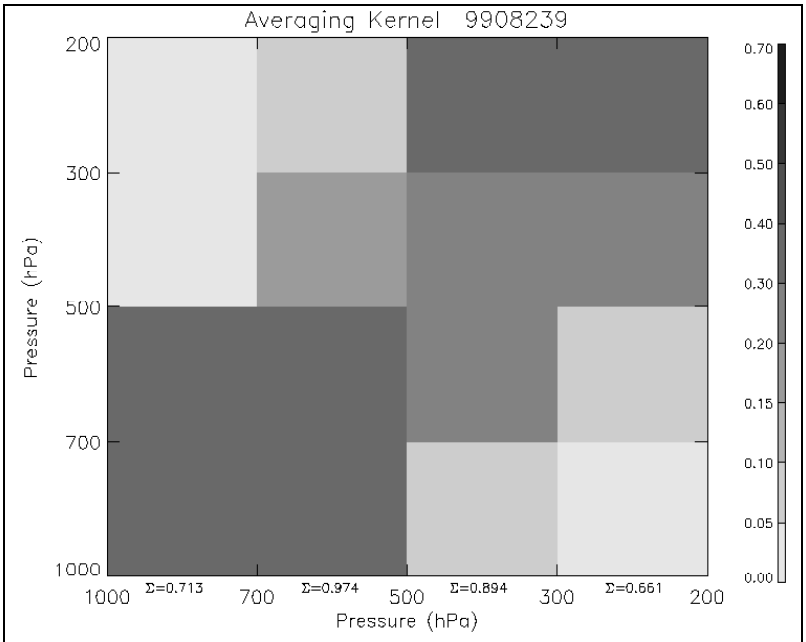

Fig. 5.23 Same as Fig 5.17, but for August 27, 1999.

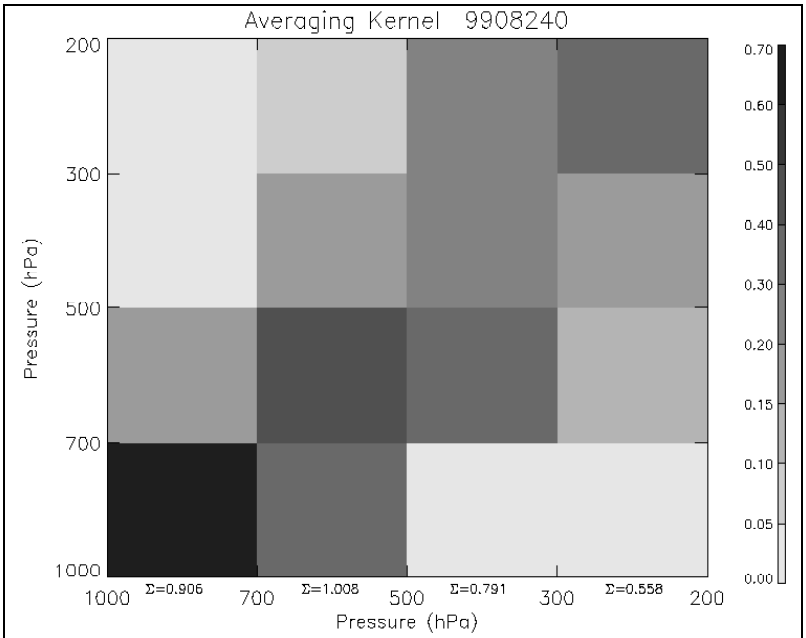

Fig. 5.24 Same as Fig 5.17, but for August 28, 1999.

To assess whether the measurements are consistent with the errors, a parameter χ^2 is defined such that

$$\chi^2 = \{y - F(\hat{x})\}^T S_y^{-1} \{y - F(\hat{x})\} + \{x_a - \hat{x}\}^T S_a^{-1} \{x_a - \hat{x}\} \approx 2 \qquad (5.2)$$

(where $2 = \#layers_{measured} + \#layers_{virtual} - \#layers_{retrieved} = 3 + 3 - 4$), and ranges between 0.1 and 1.0 with a mean of 0.53 for the eight case study days (not shown). The mean of 0.53 compared to the "expected" value of 2 implies that either the measurement covariance (S_y) was set too large or the *a priori* constraint (S_a) is slightly too loose (Marks and Rodgers 1993).

5.2.2 Errors Associated With HIRS/2

The inherent errors associated with satellite soundings will not be addressed here; an excellent source for an introduction to the advantages and disadvantages of using satellite soundings is presented in Kidder and Vonder Haar (1995), while more detailed analyses can be found in Rodgers (1990), Eyre (1990), and Smith (1991). Instead, potential errors from the retrieval are the focus of this section. There are three fundamental potential sources of error: the cloud-clearing process, the spatial averaging, and the averaging of the descending and ascending passes.

Any cloud-clearing process is prone to error because of the uncertainty in defining a cloud in a digital pixel array. This is not necessary a fault of the method (Rossow and Garder 1993), but of current technology. Thin cirrus (or "invisible" cirrus) are especially difficult to detect and sub-pixel-scale clouds present a large challenge as well. If a pixel is identified as cloudy, it is replaced with a known "clear" pixel. However, if it is not identified as cloudy, either the pixel actually is clear or there are clouds not being seen. It is the latter case that is the potential source of error in this study.

Secondly, spatial averaging is always a concern when working with satellite data. Recall from Section 2.2 that the HIRS/2 instrument has a horizontal resolution, or footprint, of 42 km. The aircraft data were compiled from a region approximately 145 km in diameter (centered over Louisville, KY). The satellite data points were taken from the exact latitude and longitude of Louisville, but that point is only a small section of a much

larger footprint. The spatial averaging used in obtaining the footprint is a factor that cannot be ignored.

Thirdly, and more importantly, is the averaging of satellite passes over a given location, i.e., temporal averaging. The NOAA-14 satellite passed over the study area twice per day, descending (traveling equatorward) at 0928 UTC, and ascending (traveling poleward) at 2128 UTC (Kidder 2000). The HIRS/2 files processed by Bates and Jackson (Section 2.2) contained a daily average of radiances; that is, the two passes each day were averaged together. Although this does make many tasks easier, it reduces the accuracy and uniqueness of a single pass. Water vapor features, like the weather, are transient and can exhibit very fine details. For example, a dry plume or moist plume may have been in place over Louisville during one pass, but an entirely different air mass could have replaced it twelve hours later. Figure 5.25 shows the variation of specific humidity (water vapor mixing ratio) over Louisville, KY during August, 1999. Using WVSS data, the plot shows that on five of the case study days (01Aug, 05Aug, 20Aug, 27Aug, and 28Aug), there was slight to moderate drying between the first satellite overpass at 0928 UTC and the second overpass at 2128 UTC; on two days (25Aug and 26Aug) there was very little change; and on one day (06Aug) there was moistening in the upper levels.

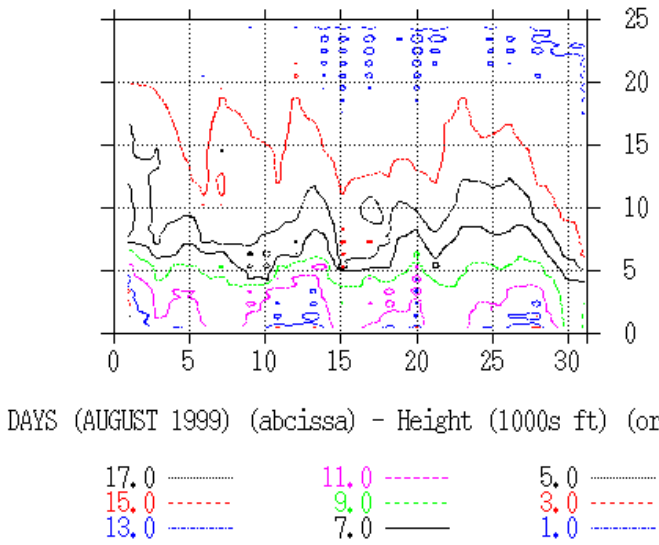

Fig. 5.25 Diagram showing the temporal variation of specific humidity (water vapor mixing ratio) over Louisville, KY during the entire month of August 1999. The ordinate scales from 1000 hPa (0 km) to 380 hPa (25 km)(Fleming 2001c).

To partially account for the effect of satellite pass averaging, all aircraft soundings over Louisville during a given day were utilized, creating an average of those as well. The end result is a reasonably accurate comparison of the daily-average precipitable water profile.

Furthermore, a daily average temperature profile (computed from a large sample of ACARS temperature measurements over Louisville, KY) was input to the retrieval so it could more accurately convert radiances to brightness temperatures (or equivalent blackbody temperature). However, a daily average temperature profile yields a more uncertain radiation profile because of Planck's Law:

$$B_\lambda(T) = \frac{2hc^2}{\lambda^5\left(\exp\left(\frac{hc}{k_B\lambda T}\right)-1\right)}, \tag{5.3}$$

where B is the blackbody radiation, h is Planck's Constant (6.62 x 10^{-34} J s), c is the speed of light in a vacuum (2.99 x 10^{8} m s^{-1}), λ is the wavelength of the radiation, k_B is Boltzmann's Constant (1.38 x 10^{-23} J K^{-1}) and T is the emitted temperature. An example of how two similar temperatures can yield two more diverse blackbody measurements is presented in Figure 5.26.

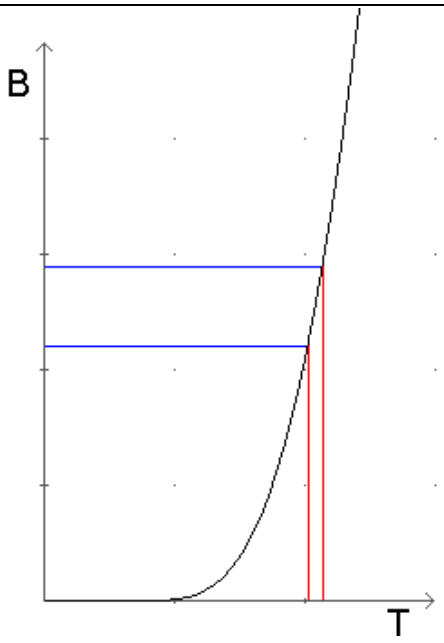

Fig. 5.26 A graph demonstrating Planck's Law: $B \propto e^{T}$. Two similar temperatures are shown in red, and the corresponding radiance measurements are shown in blue.

5.2.3 Errors Associated With WVSS

One of the principle reasons WVSS was chosen for the "truth" data in this study is its accuracy. Fleming and Braune (2000) advertise an error of 5-15% in relative humidity for an impressively large temperature range (25°C to –40°C). This translates to a fairly small, but variable, error in mixing ratio. According to the definition of relative humidity:

$$RH = \frac{w}{w_s}, \tag{5.4}$$

larger errors are likely for drier air and smaller errors are likely for moister air (here, w is the mixing ratio and w_s is the saturation mixing ratio). In practice, error in RH is approximately 5% during ascents and descents and approximately 10-15% *en route*. The random error is caused by dynamic heating; the same phenomenon which allowed the instrument to perform well at cold temperatures. Dynamic heating in the measurement chamber greatly reduces the RH in the chamber. Correcting for that artificial drying causes errors to be greater when aircraft speed is faster (higher altitude) and when the ambient temperature is colder, as seen in Figure 5.27.

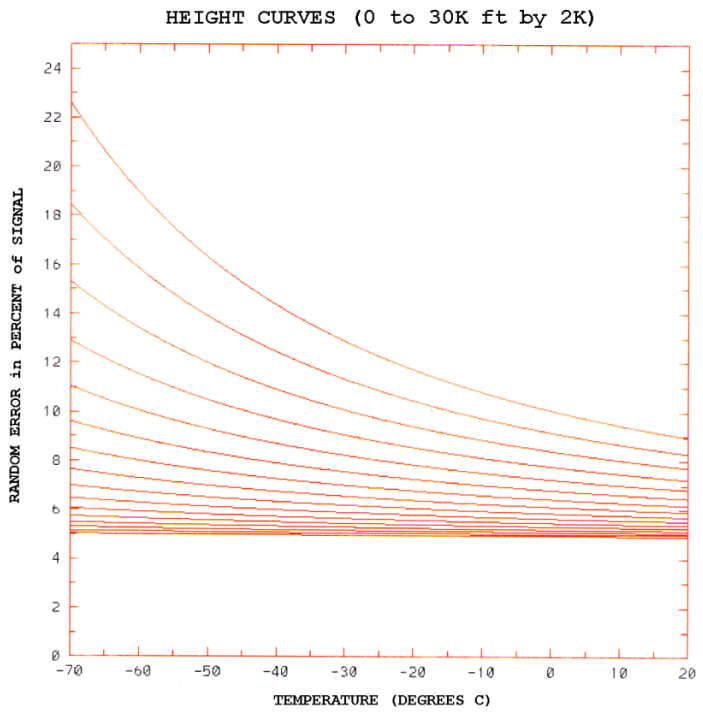

Fig. 5.27 Random error in percent of signal for the WVSS as a function of temperature and as a function of height. The height curves start at the bottom at 0 ft (~1000 hPa) and then each subsequent curve is 2,000 ft higher until the top curve of 30,000 ft (~300 hPa)(Fleming and Braune 2000).

5.2.4 Sounding Errors

Taking the previously described errors into account, the following plots show the relative and absolute differences between ACARS measured and HIRS/2 retrieved precipitable water. The data points shown in each figure are the result of averaging all eight case study days together. Although Figures 5.1-5.8 generally showed a dry bias for HIRS/2, Figures 5.28 and 5.29 definitively demonstrate a dry bias for the HIRS/2 water vapor retrieval. It is important to note that the top point in both plots (corresponding to the 200-300 hPa layer) is not a representative average. There were only three cases (20Aug, 25Aug, 28Aug) where the ACARS sounding reached high enough to collect data at that altitude. Therefore, the quality of the average is minimal and should not be weighted too heavily. However, all eight cases did factor into the averages for the lowest three points in the figures.

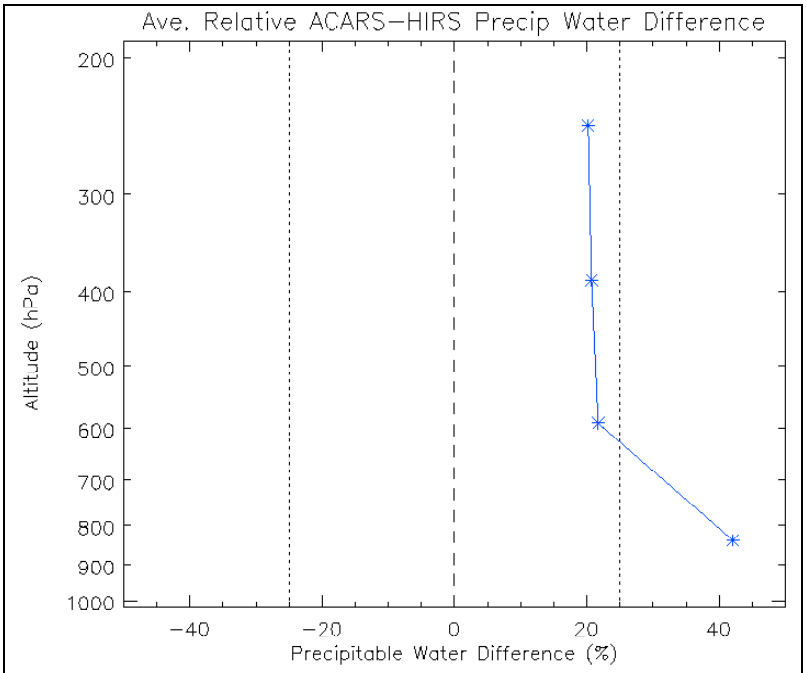

Fig. 5.28 Average relative error (percent) between the ACARS and HIRS/2 profiles. The average was calculated using all eight case study days. A positive difference means that the retrieved HIRS/2 profile is drier than the measured ACARS profile.

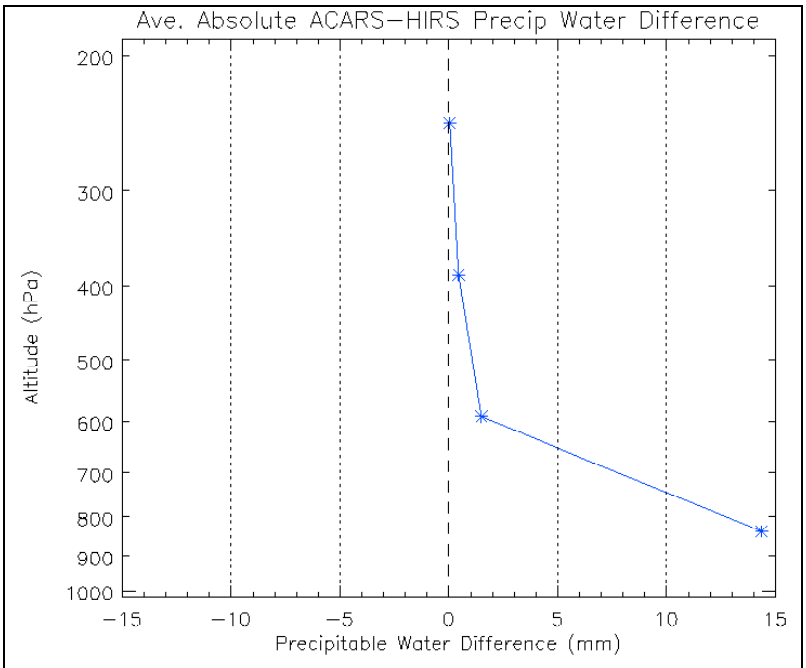

Fig. 5.29 Average absolute error (mm) between the ACARS and HIRS/2 profiles. The average was calculated using all eight case study days.

The bias is amazingly uniform through the atmosphere. The water vapor retrieval tends to underestimate the moisture content by about 20% through the bulk of the atmosphere, and by about 40% near the surface. In terms of absolute error, WVSS is wetter by about 14.4 mm near the surface (0-3 km), 1.5 mm in the 700-500 hPa layer (3-5.5 km), 0.4 mm in the 500-300 hPa layer (5.5-9 km), and only 0.04 mm in the 200-300 hPa layer (9-12 km).

The general pattern of error agrees well with the findings of Engelen and Stephens (1999) in that the retrieval algorithm performs fairly well in the upper troposphere, but not as well in the lower troposphere.

6. Conclusions

Aircraft provide the unique ability to actually go to the place in the atmosphere where one desires a measurement, then take one *in situ*. Satellites, on the other hand, are far outside the bulk of the atmosphere and can only observe the radiation coming from the planet's gaseous envelope. It is up to the satellite users to correctly calibrate, interpret, and transform the measured radiances into useful quantities, such as precipitable water, for example. Satellites will continue to prove valuable because of the quantity of information gained from them, but the ability to understand and fully utilize their information will make them priceless.

6.1 Interpretation of Results

The results presented in Chapter 5 are not totally conclusive, but they do provide the first comparison between the HIRS/2 water vapor retrieval and actual *in-situ* measurements made by a new quasi-operational aircraft system. One needs to keep in mind that the study was only performed over one site during one month of one year.

The novelty of the WVSS program and the uniqueness of the pre-processed HIRS/2 radiances at the time of conducting the research are largely responsible for constraining the scope of the study. In August 1999, there were only six WVSS sensors in operation, all mounted on United Parcel Service planes. In order to acquire multiple soundings each day, UPS's headquarters in Louisville, Kentucky was chosen as the site over which all validations would be done. The HIRS/2 pre-processing had just begun at NOAA/ETL, so special accommodations were made to provide the radiances from August 1999.

Possible sources of error included an imperfect cloud-clearing algorithm, satellite footprint averaging (spatial), overpass averaging (temporal), and from the aircraft, the largest error arises from correcting for dynamic heating.

It was shown that the Forward Model correctly processed the measured radiances by differencing the measured and modeled radiances then comparing the result to the prescribed errors, or measurement covariance. Furthermore, by making use of the averaging kernel, one can see that the retrieval did not merely regurgitate the *a priori* data. The retrieval was most sensitive to water vapor in the 500 – 700 hPa layer followed closely by the 300 – 500 hPa layer, which is in fair agreement with the findings of Engelen and Stephens (1999). This research indicates that there is a 20% dry bias to the retrieved soundings when compared to soundings made by the Water Vapor Sensing System.

Should the HIRS/2 data be used in operational forecast models, or even long-term climate research, the forecaster or researcher needs to know how to correctly interpret the results, and to not always naïvely accept them as truth.

6.2 Future Work

This research was deliberately chosen as an early test of two new water vapor datasets: the HIRS/2 pre-processed radiances and the aircraft-based Water Vapor Sensing System. Both platforms are expanding (for example, HIRS/3 has since been implemented and WVSS-II is on the horizon), so additional comparisons will shortly be possible.

Many aspects of suggested future work are mentioned in Section 4.2, but a broader overview will be presented here. It is critical to reiterate that this study is one of the first of its kind and is therefore very preliminary and focused. Fundamental factors that need to be overcome before more work is done are 1) the expansion of the WVSS program

and 2) the processing of more recent HIRS/2 data to coincide with the newer and more numerous WVSS measurements. These two upgrades must both occur to broaden the scope of this validation study. The satellite data processing is largely a manpower issue and is not as difficult to overcome, but the growth of the WVSS program depends on funding, success, and airline cooperation.

The methodology used here could easily be expanded to utilize a larger WVSS program, allowing for “validations” to be performed over oceans, mountains, and deserts. It could also be done in various climate regimes, or during warm and cold seasons over a single location. Only then can the water vapor retrieval algorithm be robustly and satisfactorily validated. It is hoped that this study will provide a launch pad to such future work.

7. References

Benjamin, S.G., D. Kim, and T.W. Schlatter, 1995: The Rapid Update Cycle: A New Mesoscale Assimiliation System in Hybrid Theta-Sigma Coordinates at the National Meteorological Center. Preprints: Second International Symposium on Assimilation of Observations in Meteorology and Oceanography, Tokyo, March 13-17, 1995, 337-342.

Berg, W., J.J. Bates, and D.L. Jackson, 1999: Analysis of Upper-Tropospheric Water Vapor Brightness Temperatures from SSM/T-2, HIRS, and GMS-5 VISSR. *Journal of Applied Meteorology*, **38**, 580-595.

Bréon, F.-M., D.L. Jackson, and J.J. Bates, 2000: Calibration of the Meteosat Water Vapor Channel Using Coincident NOAA/HIRS-12 Measurements. Submitted, *Journal of Geophysical Research*.

Engelen, R.J., and G.L. Stephens, 1999: Characterization of Water Vapor Retrievals from TOVS/HIRS and SSM/T-2 Measurements. *Quarterly Journal of the Royal Meteorological Society*, **125**, 331-351.

Engelen, R.J., and G.L. Stephens, 1998: Comparison Between TOVS/HIRS and SSM/T-2 Derived Upper-Tropospheric Humidity, *Bulletin of the American Meteorological Society*, **79**, 2748-2751.

Engelen, R.J., and G.L. Stephens, 1997: Infrared Radiative Transfer in the 9.6-μm Band: Application to TIROS Operational Vertical Sounder Ozone Retrieval. *Journal of Geophysical Research*, **102**, 6929-6940.

Eyre, J.R., 1990: The Information Content of Data from Satellite Sounding Systems: A Simulation Study. *Quarterly Journal of the Royal Meteorological Society*, **116**, 401-434.

Fleming, R.J., 1996: The Use of Commercial Aircraft as Platforms for Environmental Measurements. *Bulletin of the American Meteorological Society*, **77**, 2229-2242.

Fleming, R.J., 1999: Water Vapor Sensing System Program. http://www.joss.ucar.edu/wvss/.

Fleming, R.J. and C.E. Braune, 2000: Background Information on the First-generation, Real-time Water Vapor Sensing System for Commercial Aircraft. UCAR Technical Report, 33pp.

Fleming, R.J., personal communication, January 16, 2001(a).

Fleming, R.J., personal communication, February 1, 2001(b).

Fleming, R.J., personal communication, March 19, 2001(c).

Jackson, D.L. and G.L. Stephens, 1995: A Study of SSM/I-Derived Columnar Water Vapor Over the Global Oceans. *Journal of Climate*, **8**, 2025-2028.

Kidder, S.Q. and T.H. Vonder Haar, 1995: *Satellite Meteorology: An Introduction*. Academic Press, 466pp.

Kidder, S.Q., personal communication, July 6, 2000.

Kley, D., personal communication, January 12, 2001.

Lorenc, A.C., D. Barker, R.S. Bell, B. Macpherson, and A.J. Maycock, 1996: On the Use of Radiosonde Humidity Observations in Mid-latitude NWP. *Meteorology and Atmospheric Physics*, **60**, 3-17.

Marenco, A., 1998: Measurement of Ozone and Water Vapor by Airbus in-service Aircraft: The MOZAIC Airborne Program, An Overview. *Journal of Geophysical Research*, **103**, 25631-25642.

Marks, C.J. and C.D. Rodgers, 1993: A Retrieval Method for Atmospheric Composition From Limb Emission Measurements. *Journal of Geophysical Research*, **98**, 14939-14953.

Newell, R.E., 2000: Validation Studies for AIRS Using MOZAIC Data. Unpublished.

NOAA (National Oceanic and Atmospheric Administration), NASA (National Aeronautics and Space Administration), and USAF (United States Air Force), 1976: *Standard Atmosphere*. United States Government Printing Office, 227 pp.

Randel, D.L., T.H. Vonder Haar, M.A Ringerud, G.L. Stephens, T.J. Greenwald, and C.L. Combs, 1996: A New Global Water Vapor Dataset. *Bulletin of the American Meteorological Society*, **6**, 1233-1246.

Rodgers, C.D., 1976: Retrieval of Atmospheric Temperature and Composition From Remote Measurements of Thermal Radiation. *Review of Geophysical and Space Physics*, **14**, 609-624.

Rodgers, C.D., 1990: Characterization and Error Analysis of Profiles Retrieved From Remote Sounding Measurements. *Journal of Geophysical Research*, **95**, 5587-5595.

Rossow, W.B. and L.C. Garder, 1993: Cloud Detection Using Satellite Measurements of Infrared and Visible Radiances for ISCCP. *Journal of Climate*, **6**, 2341-2369.

Smith, W.L., 1991: Atmospheric Soundings From Satellites – False Expectation or the Key to Improved Weather Prediction? *Quarterly Journal of the Royal Meteorological Society*, **117**, 267-297.

Stephens, G.L., D.L. Jackson, and I.L. Wittmeyer, 1996: Global Observations of Upper-Tropospheric Water Vapor Derived from TOVS Radiance Data. *Journal of Climate,* **9**, 305-326.

Stephens, G.L., 1994: *Remote Sensing of the Lower Atmosphere*. Oxford University Press, 523 pp.

Susskind, J., J. Rosenfield, D. Reuter, and M.T. Chahine, 1984: Remote Sensing of Weather and Climate Parameters From HIRS2/MSU on TIROS-N. *Journal of Geophysical Research*, **89**, 4677-4697.

Susskind, J., P. Piraino, L. Rokke, L. Iredell, and A. Mehta, 1997: Characteristics of the TOVS Pathfinder Path A Dataset. *Bulletin of the American Meteorological Society*, **78**, 1449-1472.

Vonder Haar, T.H., J.M. Forsythe, D.L. Randel, and R.J. Engelen, 1999: Comparison of a New TOVS Upper Tropospheric Moisture Retrieval With Other Water Vapor Datasets. Preprints, *10th Conference on Atmospheric Radiation*, Madison, WI, American Meteorological Society, 244-247.

Wagoner, S.M., personal communication, October 26, 2000.

Wallace, J.M. and P.V. Hobbs, 1977: *Atmospheric Science: An Introductory Survey*. Academic Press, 467 pp.